Aalto University
School of Chemical
Technology

School of Chemical Technology
Degree Programme of Bioproduct Technology

Wenchao Xiang

Silver Nanoparticles Formation on Fibres and Potential for Optical Sensing

Master's thesis for the degree of Master of Science in Technology submitted for inspection, Espoo, 27, October, 2014.

Supervisor Professor Orlando Rojas

Instructor Dr. Lokanathan Arcot

Aalto University
School of Chemical
Technology

Aalto University, P.O. BOX 11000,
00076 AALTO
www.aalto.fi

Abstract of master's thesis

Author Wenchao Xiang

Title of thesis Silver Nanoparticles Formation on Fibres and Potential for Optical Sensing

Department Forest Products

Professorship Forest Products Chemistry **Code of professorship** Puu-19

Thesis supervisor Prof. Orlando Rojas

Thesis advisor(s) / Thesis examiner(s) Dr. Lokanathan Arcot

Date 27.10.2014 **Number of pages** 56 **Language** English

ABSTRACT

Silver nanoparticles (AgNP) formation mediated by fibres in paper can be a promising process for optical sensing applications with high sensitivity and low cost. Thus, the aim of this thesis was to develop a paper-based sensor to quantify the concentration of analyte. The work focused on investigating the role of interactions between silver ions-cellulosic hydroxyl groups and analyte molecules in AgNP formation.

A multilayer sensor module that included layers supporting silver ion precursor and ascorbic acid reducing agent was constructed. The effect of positional order of the sensor layers on AgNP formation was studied. UV-vis spectroscopy and SEM were used to characterize the AgNP plasmon effect and morphology, respectively. Initially, cationic (DDAB), anionic (SDS), and nonionic (Triton X) surfactants were used as model analytes carrying different electrostatic charges. Further investigation was performed with biomolecules including cholesterol, BSA, gamma-globulin.

UV-vis absorption results of sensor modules with varied layer-order confirmed the pivotal role of cellulosic hydroxyls in AgNP nucleation and growth processes, which were characterized by the two typical plasmonic peaks located at short and long wavelengths (~420 and 500~600 nm, respectively). Compared with the nonionic and the surfactant-free conditions, the cationic and anionic surfactants yielded more uniform and reproducible results in terms of AgNP formation and respective plasmon signal. The investigation with cholesterol confirmed main findings with surfactants by revealing distinct blue shifts in the long wavelength plasmonic peaks. However, the results with BSA and gamma-globulin proteins were inconclusive due to the possible the interference of impurities or other causes not yet identified.

The findings in this thesis not only are consistent with previous studies, but also highlight opportunities for sensor design based on AgNP formation process instead of traditional platforms based on pre-synthesized AgNP. Further work will be needed to understand the mechanism of blue shift caused by the analyte and to optimize its correlation with concentration in the presence of interfering substances.

Keywords paper sensor, silver nanoparticles, cellulose hydroxyl, surface plasmon resonance, UV-vis absorption

ACKNOWLEDGEMENT

This thesis work was completed in the Department of Forest Products.

I would like to thank Prof. Janne Laine for generously accepting me into his research group to start my thesis. His intelligent and humorous speeches, as well as inspiring talks from the other group members are valued.

My enormous thanks belong to my thesis instructor Dr. Lokanathan Arcot, who is always there for discussing and answering all my questions. He opened the door of quantum confinement to me, and guided me to step into the world of “smart” materials. It is priceless to have learned from and worked with him.

I wish to give my sincere thanks to Prof. Orlando Rojas for his helpful guidance. Without that, my master`s thesis and defense would not have been fulfilled eventually.

Lastly, my genuine thanks go to my beloved parents, my grandmother, and my friends, “inside and outside Aalto”. Their unconditional love and trust have helped me to find a better version of myself, and supported me to explore the world freely like a horse.

Espoo, 27 October, 2014

Wenchao Xiang

CONTENTS

1 BACKGROUND

This thesis project is a proof-of-concept study bridging fundamental understanding and biosensing applications. To lay a solid understanding of this interdisciplinary project work, this section covers essential information to motivate our proposed application potential. Additionally, the rationale behind the choice of model analyte molecules systems shall be covered subsequently.

1.1 Silver Nanoparticles (AgNP)

Modern research has witnessed the development of highly sensitive, selective and robust detection methods. Advances in nanotechnology have facilitated the development of novel biosensors. Of interest in this field are the so-called plasmonic nanoparticles, which include silver nanoparticles (AgNP), also known as colloidal silver, which have at least one dimension chiefly in 1~100 nm (Mohd et al., 2011). AgNP have attracted enormous interests in the sensors research community mainly due to its distinct optical, electrical, antibacterial and thermal properties. Besides, these surface dependent properties resulted from extremely high surface-to-volume ratio of AgNP, do not apply to bulk silver.

Owning to these unique properties, AgNP have found numerous applications in developing biosensor materials (Jeffery et al., 2008; Ren et al., 2005; Adam et al., 2003), cryogenic superconducting materials (Hirano et al., 2002), antimicrobial systems (Xiu et al., 2012; Manash et al., 2011; Stephan et al., 2006; Ivan & Branka, 2004), cosmetic products (Tian et al., 2006), and composite fibers (Minwoo et al., 2012; Hong et al., 2006; Son et al., 2006), etc. In terms of applications derived from optical properties, all developments are based on AgNP`s plasmon effect. Therefore, theoretical aspects of such effect will be introduced in the following section.

1.1.1 Basis of optical property: surface plasmon

Most explorations of applications and innovations in bio-sensing and detecting areas stem from the peculiar optical properties of AgNP, which originate from the surface plasmon resonance (SPR) effect. To illustrate SPR, the surface of a metallic nanoparticle is like plasma, comprising free electrons in the conduction band on the surface and positively charged nuclei in the core. Under the influence of an alternating electric field of incident light of certain wavelength/frequency, these mobile conduction electrons are excited, leading to a collective oscillation, namely, SPR (Kreibig & Vollmer, 1995) (figure 1.1). This strong oscillation causes an effective extinction (scattering + absorption). AgNP exhibits the highest extinction ratio, compared to all the other metallic nanoparticles, as well as other materials that absorb in the same spectral region (Yu et al., 2008). Additionally, AgNP plasmon modes raise strong absorption in the UV-vis spectral region (Vesna et al., 2008), which can be quantified by spectroscopy techniques with distinct plasmon peaks as indications.

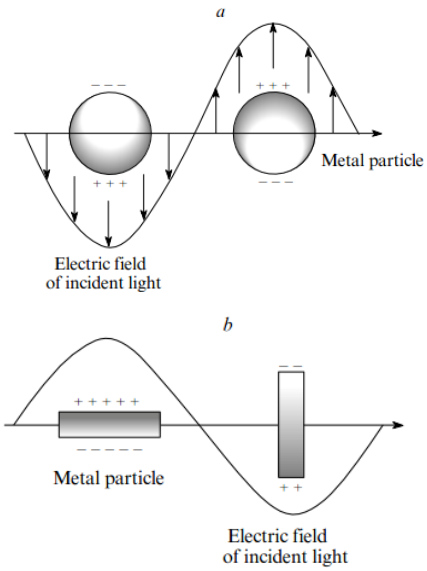

Figure 1.1. Scheme of surface plasmon oscillation under the effect of electromagnetic field: (a) spherical particle, (b) cylindrical particle (Yu et al., 2008).

The energy and mode of vibrations of surface free electrons are dependent on both particle (size, shape, number, agglomeration state) and the surrounding environment. The characteristic plasmon bands exhibited in UV-vis spectroscopy will vary correspondingly. To be specific, the increment in particle number and size will lead to an increased plasmonic peak intensity. Additionally, as the particle diameter increases, the single, narrow SPR absorption peak due to the dipole plasmonic oscillation (figure 1.2A) will shift towards higher wavelength values, also known as "red shift". A more monodisperse size distribution of AgNP will result in narrower or sharper UV-vis plasmon peak. Plasmon peak asymmetry, especially towards the long wavelength region is indicative of the presence of aggregates formed by uncontrolled growth and stabilization. Large AgNP aggregates formed by aggregation or coalescence exhibit higher order plasmonic oscillation modes including quadrupole and octupole oscillations, etc. (figure 1.2B, C), leading to several peaks (Tricker et al., 1970; Prashant et al., 1998) (figure 1.3). Apart from the effects of particle number, size, agglomeration, unique plasmon bands will also occur due to the changes in particle shapes (figure 1.4) (Xia et al., 2009). Moreover, the influence of particle`s surrounding environment was demonstrated by Vesna and co-workers in 2008. By transferring spherical AgNP (d=5.6 nm) synthesized in polar solvent (water) using $NaBH_4$ as reducing agent into non-polar solvent (chloroform) with oleylamine (as phase transfer reagent), the AgNP was found to have a stronger absorption spectrum, with a 19 nm red shift compared to that for particles in water.

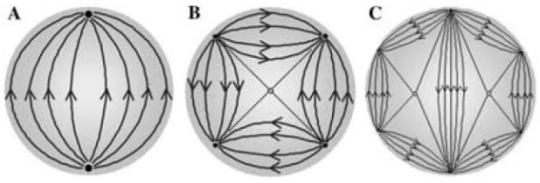

Figure 1.2. Diagrams of (A) dipole, (B) quadrupole, and (C) octupole resonances (David et al., 2005).

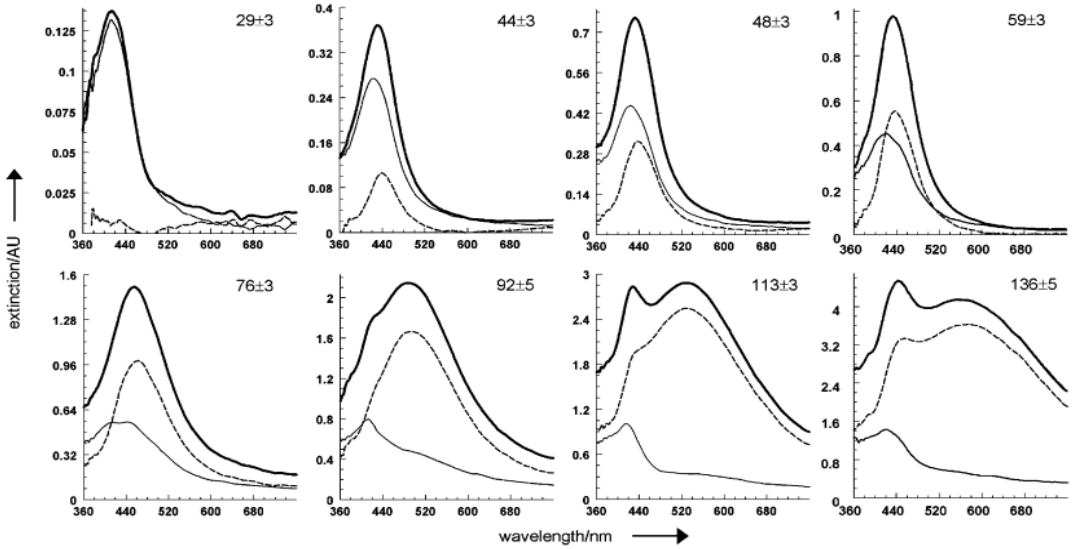

*Figure 1.3. Extinction (**–**), scattering (---), and absorption (–) spectra of silver nanoparticle suspensions normalized per particle. The mean particle sizes are noted in each panel. The units on the y axis are multiplied by 10 (Lee et al., 1982).*

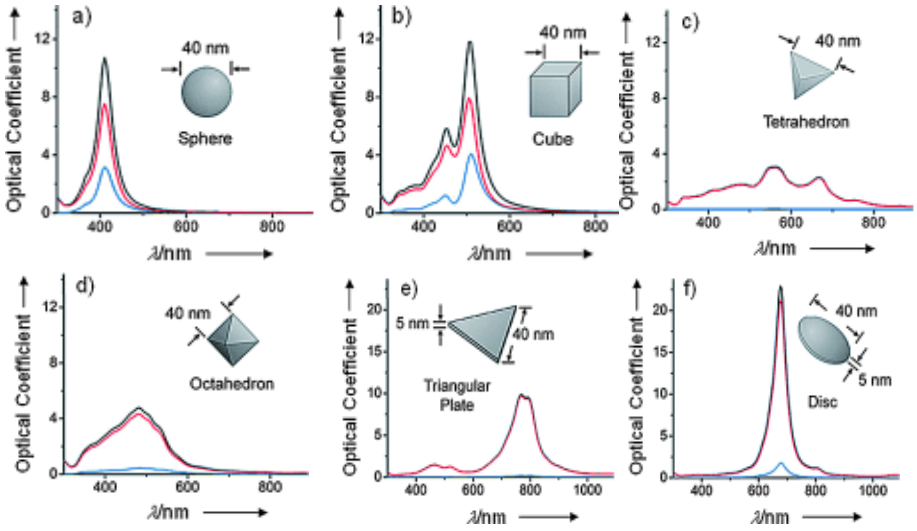

Figure 1.4. Calculated UV-visible extinction (black), absorption (red), and scattering (blue) spectra of Ag nanocrystals, illustrating the effect of shape on spectral characteristics: a) sphere, b) cube, c) tetrahedron, d) octahedron, e) triangular plate, and f) circular plate (Xia et al., 2009).

1.1.2 Sensing applications based on optical properties

Numerous sensing applications of AgNP have been developed based on the utilization of SPR properties. All reported plasmonic sensing applications can be classified into two main categories (Carlos et al., 2010). Namely, a frequency shift dependent sensing, which can further be subdivided into aggregation based frequency shift (known as aggregation sensor) and surrounding refractive index change based frequency shift (known as refractive sensor). The second type involves electromagnetic field enhancement in the vicinity of AgNP or otherwise known as surface enhanced spectroscopy.

For instance, Wei and co-workers developed a colorimetric assay to monitor the enzymatic reactions, which, in their case, involved the consumption of adenosine triphosphate (ATP) in enzymatic reactions. The mechanism is based on following the salt induced aggregation of AgNP, caused by the diminished protection from ATP, which is consumed in the enzymatic reactions, such as, ATP dephosphorylation by calf intestine alkaline phosphatase (Wei et al., 2008). A refractive index sensor using silver colloidal nanoparticles to detect pollutant, such as volatile organic compounds, was reported by Chen et al. (Chen & Lu, 2009).

The electromagnetic field enhancement can be illustrated by surface enhanced spectroscopies, namely, metal enhance fluorescence (MEF) and surface enhanced Raman spectroscopy (SERS). SERS is probably the most powerful tool currently available for sensing, due to its extremely high sensitivity derived from its ability to detect a molecule located close to a nanoparticle (Carlos et al., 2010). With this intention, a new powerful tool, known as SERS tags functioning as chemically encoded labelling agents, has emerged. Specifically, the fundamental structure of a SERS tag is the labelling agent, known as SERS reporter molecule, which has a high Raman cross section and can be selectively further wrapped in a protective shell after being absorbed on the surface of a AgNP. For detection purposes, this basic structure can be conjugated to a recognition element, like an antibody. For

example, Xia et al. reported a new SERS tag for imaging cancer cells by fabricating sequentially functionalized dimers, produced from 50 nm AgNP with 4-mercaptobenzoic acid as the Raman reporter molecule, and silica coating as the protective shell, as well as antibody as the targeting ligand. The potential utilization of their SERS tags was demonstrated with good specificity and high sensitivity by imaging cancer cells overexpressing HER2 receptors (Xia et al., 2013). Additionally, MEF also plays a major role in many biological assays, based on the fact that MEF can lead to 10~1000 fold intensity enhancement (Yi et al., 2012; Mustafa et al., 2011).

To summarize, based on the utilization of pre-synthesized AgNP, the exploration of their optical properties has opened the door to advances in sensing applications, though the related pre-synthesis process itself is mostly sophisticated.

1.1.3 Typical characterization techniques

The size, shape and morphology of AgNP are typically characterized by techniques including transmission electron microscopy (TEM), scanning electron microscopy (SEM) and atomic force microscopy (AFM). In some cases, dynamic light scattering (DLS) or analytical disc centrifugation have been used for measuring the aggregation state of particles in solution (Zhang et al., 2000; Geert et al., 2012). Nevertheless, due to the unique optical property of AgNP, a great deal of information of physical state of AgNP can be obtained from UV-vis spectroscopy, which is a valuable tool in most studies. Accordingly, in this thesis project, UV-vis spectroscopy was used as the main characterization technique. As a supplementary technique for further understanding, SEM was also applied.

1.2 Role of Cellulose in AgNP Green Synthesis

Driven by the progress in the field of AgNP related applications, its synthesis by physical, chemical and biological approaches has been widely developed. Two representative physical approaches are evaporation-condensation (Jung et al., 2006) and laser ablation (Takeshi et al., 2008). As the most common approach for synthesis, chemical reduction has been deeply explored. Representative inorganic and organic redox reductions include those between sodium borohydride ($NaBH_4$) (Tolaymat et al., 2010) and silver salts, and the Tollens reaction (Ruggero et al., 2012), respectively. The popularity of $NaBH_4$ is due to the relatively high reactivity of borohydride compared to other reducing agents, and relatively handy protocols compared to physical methods, as well as relatively low toxicity compared to hydrazine and hydroxylamine. Besides, the mechanism of borohydride reduction is well understood. Efficient as these approaches are, most physical and chemical reactions do not involve eco-friendly reducing agents and stabilizers. As part of the sustainable strategy, biosynthesis methods have been proposed. Amidst these alternatives, green synthesis approaches with renewable materials, such as carbohydrate or cellulose based materials, have drawn special attention, owning to their advantages over microorganism cultured synthesis, which can also be considered to be a quasi-biosynthesis approach. For instance, comparing to microorganisms processes, synthesis with carbohydrate-/cellulose- based materials will be more suitable for scaling up by avoiding the cell culture processes (Song et al., 2009), and by faster and more stable synthesis (Iravani, 2011).

Cellulose, as the most abundant natural polymer (Gilberto et al., 2010), has opened a land of opportunities for applications from nano-scopic (i.e. cellulose nanocrystals (CNC), cellulose nanofibers (CNF), bacterial cellulose (BC)) to macro-scopic fiber-based materials including paper. Apart from its biodegradable and renewable properties, the popularity of cellulose significantly depends on its intrinsic structure which consists of cellobiose as the basic repeating unit, together with reducing and non-reducing ends. Importantly, due to the abundant hydroxyl groups along the cellulose chains, numerous functionalization for diverse purposes can been

achieved. Given that, cellulose is believed to influence AgNP formation via ion-dipole interaction between silver ions and cellulosic hydroxyls, and/or through surface passivation of AgNP by polysaccharide-metal surface interactions.

The role of hydroxyl groups or charges from modified cellulose surfaces is especially important when CNC is under consideration. By taking advantage of this Rui et al. demonstrated for the first time the capability of CNC to synthesis dendritic AgNP in a relative mild condition (under 100°C with water as a medium), without adding any other reductant, stabilizer, or capping agent (Rui et al., 2013). Moreover, Nicolas and co-workers generated spherical AgNP in mild alkaline conditions by using the reducing power of CNCs introduced via periodate oxidation (Nicolas et al., 2010). Besides, CNC was reported as a scaffold to facilitate AgNP synthesis by supplying a coordination effect to absorb silver ions and AgNP (He et al., 2010 a; b).

Promising as CNC is, a well-established mechanism of the relation between CNC surfaces and AgNP nucleation and growth is lacking. Arcot and co-workers attempted an exploration of the mechanism by recording AgNP formation with varied presence of CNC through systematic desulfation (Arcot et al., 2014). As a conclusion, the nucleation controlling capability of cellulosic hydroxyls on CNC was confirmed. Furthermore, intending to explore and confirm the role of CNC surface in AgNP formation, a systematic study of formed AgNP along with corresponding presence of TEMPO oxidized CNC was performed (Khan et al., 2014). As a result, surface carboxyl groups on CNC surfaces were found to strongly influence the growth of AgNP.

Moreover, from a macro-scopic perspective, large cellulose materials, like paper, have become increasingly popular in sensing applications. One direction is to employ filter paper as SERS substrate. The validity of the choice owns to the high content of α-cellulose (98%) in filter paper, which could drastically minimize the interference from other substances. Importantly, it is observed that Whatman filter

paper #1 consists of a vast amount of micro-scale cellulose strands (~10 μm), some smaller microfibers (~0.4 μm) and nanofibers in between (Chang et al., 2011). This structure preserved the amphiphilic nature on paper surface and ensured a large surface absorption of metal ions and NPs. Based on these facts, Chang and co-workers reported a highly sensitive and reproducible SERS paper substrate, tested with gold nanorods on the surface. Additionally, with a specific concern about AgNP, Meng et al. demonstrated a rapid collection of analyte and in situ detection with AgNP decorated filter paper. In their work, AgNP were synthesized by cellulose self-sacrificing reduction, namely, by the reaction between $Ag(NH_3)_2OH$ and cellulosic hydroxyl groups in alkaline conditions. The fabricated SERS paper substrate turned out to successfully improve the Raman intensity and detection limit (Meng et al., 2013). Importantly, their work confirmed the effective potential of filter paper as a stabilizer for AgNP via Ag-O bonding interactions (He et al., 2005). Moreover, they also proved that by influencing the absorbance of analyte onto AgNP on filer paper, surface resonance of AgNP was subsequently changed.

To conclude, due to its intrinsic structure, cellulose, including nano-scopic (i.e. CNC) and macro-scopic (i.e. filter paper) matrices, is a promising ecofriendly alternative to mediate the two main processes in AgNP formation: nucleation and growth. By influencing the absorption states of among cellulose, silver, and analyte, cellulose-supported AgNP can make promising sensors, thus contributing to the developments in diagnosis and imaging, etc. with competitive detection abilities and low cost.

1.3 Motivation of the Work

Motivated by the interest to utilize AgNP for biosensing applications with high sensitivity and in a sustainable manner, a paper-based sensor was planned. Reflecting on the current progress of AgNP derived sensors, a common feature is the utilization of pre-synthesized AgNP. However, based on the introduced background information, an approach was undertaken to bring forward the

influence of analyte on the properties of AgNP upon forming on paper, which can be characterized by, for instance, UV-vis spectroscopy. In addition, another feature that was realized was the effect of molecular structure and surface chemistry of each analyte species (i.e. proteins, lipids, etc.), which can have different affinities to AgNP and paper surfaces. Thus, a hypothesis of this thesis is proposed as follows, **AgNPs with different spectroscopic properties can form on a paper-based sensor depending on the presence of a given analyte (Hypothesis 1)**.

In addition, as mentioned in the background section, paper surfaces appear to have an effective capability of interacting with silver. Nevertheless, the essential mechanism for this is not fully understood, not to mention the mechanism by which paper facilitates AgNP formation, considering the order of addition of silver ions (Ag^+) and the reducing agent. Hence, another hypothesis of this thesis work is that **paper can mediate AgNP synthesis depending on the Ag^+/reducing agent order of addition (Hypothesis 2)**.

1.4 Focus of the Work

With the ultimate goal to build a paper based sensor exploiting the AgNP forming process, it is of fundamental importance to draw conclusions on the proposed hypothesis 1 & 2. Therefore, this thesis work mainly focuses on the investigations of the role of Ag^+-cellulosic hydroxyl interactions during AgNP forming process. In addition, it explores the influence of planned analyte on the subsequently formed AgNP. Details in the approaches used will be described in the methodology section. In sum, this thesis work is of both academic and practical interest and involves the testing of a new sensor based on AgNP formation rather than pre-synthesized AgNP.

2 EXPERIMENTAL

2.1 Materials

Silver nitrate ($AgNO_3$) (≥ 99.0%), L-ascorbic acid (Re) (≥ 99.5%, RT), Triton X-100, bovine serum albumin (BSA) (≥ 98%, lyophilized powder) and magnesium sulfate ($MgSO_4$) (anhydrous, ≥ 97%) were purchased from Sigma-Aldrich. Sodium dodecyl sulfate (SDS) (≥ 99%, GC) and didodecyldimethylammonium bromide (DDAB) (≥ 99%, AT) were obtained from Fluka. Cholesterol (95%, GC) and γ-globulin (83.0%) were acquired from Calbiochem. Absolute ethanol (teknisk, ETAX Ba) was purchased from Altia Oyj. NaCl (≥ 99.9%) and $NaHCO_3$ (100.0%) were acquired from VWR. Merck supplied $CaCl_2$ (≥ 98.0%), KCl (≥ 99.5%) and KH_2PO_4 (≥ 99.5%). All chemicals were used as received, without further purification. Milli-Q water (MQ) was prepared with Synergy UV by Millipore and used for all solutions preparation, unless stated otherwise. Cellulose chromatography paper (Grade 2) was purchased from Whatman. A4 multiuse paper was purchased from Staples.

2.2 Methodology

2.2.1 3-layer sensor module design

Keeping in mind a practical utilization for blood samples, a 3-layer sensor module made from chromatography paper was designed. The chromatography paper used is typically for optical or radiometric scanning purposes and it is of high cellulose purity. In terms of the function of each layer in the sensor module, the topmost layer, denoted as ***t*** layer was included to filter microscopic substances such as blood cells. While the middle layer, which can be further modified or replaced for different purposes, was intended to filter out smaller molecules and to allow analyte molecules in solution that pass onto the bottom layer. This bottom layer, denoted

as ***b*** layer, is the place where AgNP form and thus is used for the detection of the analyte that reaches this layer. Detailed procedures for building the sensor module are as follows.

To start with, chromatography paper and A4 paper strips with a dimension of 1.5 cm × 10 cm were cut out. Then, two chromatography strips with pencil marks at 4 cm from the margins in the long dimension were prepared (figure 2.2.1). The central areas (1.5 cm × 2 cm) are the ones where either chemical addition or the redox reaction occurs. Then, one of these two strips, placed as the ***t*** layer, was fixed using staples onto a piece of A4 paper strip at 0.5 cm from the margins in the long dimension. The other piece of the marked chromatography paper strip (***b*** layer) together with a new piece of non-marked chromatography paper strip (middle layer) was inserted in the space between just stapled ***t*** layer and A4 paper strip. Importantly, the central area on the topmost chromatography paper should be located exactly above that on the b layer chromatography paper. The designed sensor module was completed after fixing together the central areas of the three chromatography paper strips with a paperclip (figure 2.2.2). It is worth noting that, the A4 paper strip used here was used just to help to construct the module structure, holding firmly the reaction area on chromatography paper strips in air, in order to avoid any attachment with other surfaces, such as the working table. Therefore, it is possible to replace the A4 paper strips with any other material that can have the same function.

The redox reaction that occurs in the sensing module involves $AgNO_3$ and ascorbic acid. In order to achieve the goal of analyte sensing via AgNP formation, before the construction of the module, $AgNO_3$ and ascorbic acid were pre-adsorbed onto the ***t*** and ***b*** layers, and using the two possible alternatives for their location or order ($AgNO_3$ and ascorbic acid each either on the ***t*** layer or on the ***b*** layer). After constructing the module, and in order to achieve the redox reaction, the analyte solution can be added onto the ***t*** layer. Thus, $AgNO_3$ or ascorbic acid is carried downwards through the middle layer towards layer ***b***. Subsequently, after sufficient time for redox reaction, the ***b*** layer can be analyzed via UV-vis spectroscopy. The

recorded UV-vis absorption spectrum is thus treated as sensing output signal. It is worth mentioning that, throughout all the experiments, $AgNO_3$ and ascorbic acid solutions were always freshly prepared before given use.

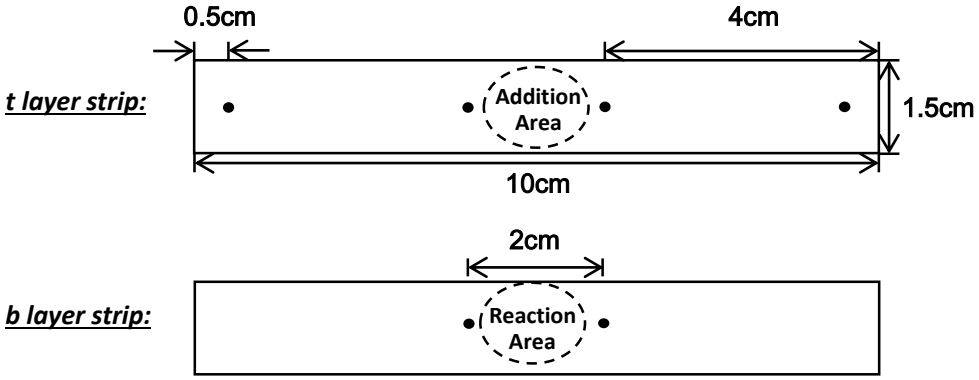

*Figure 2.2.1. Dimension illustrations of chromatography paper strips for the topmost (**t**) and bottom (**b**) layers.*

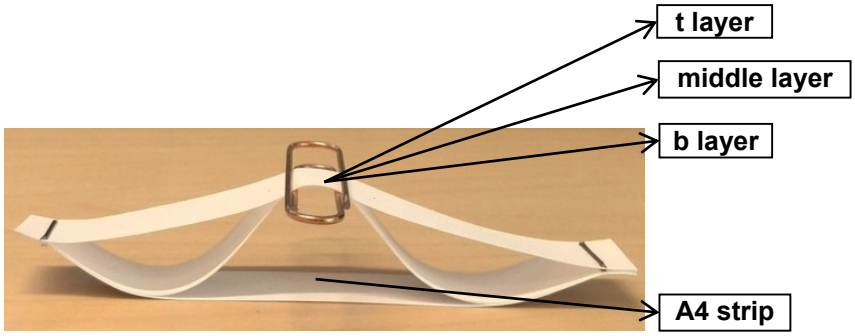

Figure 2.2.2. Photograph of constructed 3-layer sensor module structure.

2.2.2 Proof of concept studies on the 3-layer sensor module

Based on the designed 3-layer sensor module and in order to check the validity of hypothesis 2, that is, to check the effect of the addition order of silver ions/ascorbic acid to the ***b*** layer surface, modules named as *Re(**t**)Ag(**b**)* and *Re(**b**)Ag(**t**)* were constructed for comparison. Here, *Re* refers to the reducing agent and *Ag* refers to the precursor silver nitrate solution, while ***t*** and ***b*** indicate the top and bottom layers, respectively. To illustrate, in the case of *Re(**t**)Ag(**b**)* module preparation, firstly, 10 µL of 10 mM ascorbic acid and 1 mM $AgNO_3$ were added onto the ***t*** and ***b*** layers, respectively. Then these paper strips were dried in darkness at room temperature for 6 h. The *Re(**t**)Ag(**b**)* module was constructed as introduced above in 2.2.1. Finally, 40 µL of MQ representing analyte solution was applied onto the dried ascorbic acid spot. In the case of the *Re(**t**)Ag(**b**)* module, 10 µL of 10 mM ascorbic acid and 1 mM $AgNO_3$ were added onto the ***b*** and ***t*** layers, respectively, in the switched order. After constructing the module structure, 40 µL of MQ water was added on to the dried $AgNO_3$ spot, which in this case is on the topmost.

Control experiments consisted of *Ag(**b**)*, *Re(**t**)* and *Reference* modules. In these modules *Ag(**b**)* was treated with 10 µL of 1 mM $AgNO_3$ on the ***b*** layer. *Re(**t**)* was treated with 10 µL of 10 mM ascorbic acid on the ***t*** layer. In *Reference* group, nothing was applied onto each layer. As before, 40 µL of MQ water as analyte solution was added to each control group module. Table 2.2.1 presents detailed protocols for all modules. After preparing samples in duplicate, all the modules were kept in darkness during drying at room temperature for 16 h before UV-vis measurements on the respective ***b*** layer.

Table 2.2.1. Different module preparation protocols for experiments to prove hypothesis 2.

		t layer	b layer
Module Type	**Re(t)Ag(b)**	10μL of 10mM ascorbic acid	10μL of 1mM $AgNO_3$
	Re(b)Ag(t)	10μL of 1mM $AgNO_3$	10μL of 10mM ascorbic acid
	Ag(b)	--	10μL of 1mM $AgNO_3$
	Re(t)	10μL of 10mM ascorbic acid	--
	Reference	--	--

2.2.3 AgNP formation in Re(t)Ag(b) module with protein solution

BSA and γ-globulin, two important blood proteins, were used to study biomolecules detection. Instead of MQ water, the respective protein solution was used as analyte solution in this part of experiments. The working concentrations of BSA (30, 45, 60 mg/mL) and γ-globulin (7, 12, 17 mg/mL) were chosen based on normal serum albumin levels in human (35~50 serum albumin mg/mL (Corti et al., 1994) and 7~16 γ-globulin mg/mL (MedlinePlus, 2014)). To be specific, 60 mg/mL BSA and 17 mg/mL γ-globulin, were prepared as original solutions directly by dissolving proteins in MQ water. 45 and 30 mg/mL BSA, as well as 12 and 7 mg/mL γ-globulin solutions were obtained by dilution from higher solution concentrations. Each time, AgNP were formed by adding 40 μL of one kind of analyte solution to the prepared *Re(t)Ag(**b**)* module, which was constructed as described in 2.2.1. Preparation of reference group was completed by adding only 40 μL of MQ water. UV-vis measurements on ***b*** layers of these modules were done after drying in darkness at room temperature for 16 h. All sample types were prepared in duplicate. Moreover, in order to explore the effect of possible impurities in proteins including salts, experiments were carried out with salt solutions. Procedures involved here were the same as those with protein presented experiments. Since the sensor was aimed to target samples at human subjects, the salts concentration levels considered in this

study were based on the component contents in Kreb-Heneleit buffer (KHB), which resembles very closely the salt composition of serum (Tas, 2013). Detailed concentrations applied onto *Re(t)Ag(**b**)* modules are summarized in table 2.2.2.

Table 2.2.2. Working concentrations of KHB mineral salts.

NaCl (mg/mL)	0.692	6.92*	69.2
KCl (mg/mL)	0.035	0.35*	3.5
$CaCl_2$ (mg/mL)	0.028	0.28*	2.8
$MgSO_4$ (mg/mL)	0.0073	0.073*	0.73
$NaHCO_3$ (mg/mL)	0.21	2.1*	21
KH_2PO_4 (mg/mL)	0.016	0.16*	1.6

*) mineral salts concentrations in KHB (Tas, 2013).

2.2.4 AgNP formation in modified module with surfactant solution

In order to test hypothesis 1, the influence of interaction affinity on AgNP formation was investigated. In this case, a modified sensor module and model analyte solutions (cationic, anionic, nonionic surfactants) were applied. The 3-layer sensor module was substituted by only one piece of chromatography paper strip bearing a dried $AgNO_3$ (30 µL of 5 mM) spot. 30 µL of analyte solution containing 50 mM ascorbic acid and given amount of surfactant (DDAB/SDS/Triton X) was added onto the $AgNO_3$ spot (dried in darkness at room temperature for 6 h). All the prepared samples were dried in dark at room temperature for 16 h before UV-vis tests. Reference samples were completed by adding only 30 µL of 50 mM ascorbic acid. All the samples were made in triplicate.

Working concentrations of each surfactant were calculated based on the correspondingly critical micelle concentration (cmc) (table 2.2.3). The highest

concentrations of the anionic and nonionic surfactants were 90% of their cmc values to further avoid the possibility of micelle formations. One exception of the highest concentration of cationic surfactant was adjusted to 140 μM, due to the difficulty in dissolution at 90% of its cmc value. In detail, applied concentrations of DDAB were 1.4, 14 and 140 μM. As to SDS, the working concentrations were 70 μM, 0.7 and 7 mM. In the case of Triton X, they were 0.002, 0.02 and 0.2 mM. All solutions used for experiments in this section were prepared with MQ water.

Table 2.2.3. cmc values of surfactants used.

	Cationic	**Anionic**	**Nonionic**
Surfactant	DDAB	SDS	Triton X-100
cmc value / mM	13.9*	8.27**	0.22***

*) Metha et al., 2008; **) Feofanov et al., 2000 ; ***) Sigma, 2014.

2.2.5 AgNP formation in modified module with cholesterol solution

Cholesterol, as a typical lipid biomolecule in blood, was chosen for the experiments in this section. With the consideration of the solubility of cholesterol, instead of using MQ water as solvent, absolute ethanol was used. 50 mM ascorbic acid solution was firstly prepared by dissolution in absolute ethanol with the help of sonication at 25°C for 15 min. This 50 mM ascorbic acid solution was taken as reference solution, and denoted as 50 mM Re(Eth). The ascorbic acid solutions were prepared freshly before any experiment. For the sensor studies, $AgNO_3$ (5mM) attached chromatography paper strips were firstly prepared as described in 2.2.4. After drying in darkness at room temperature for 6 h, 30 μL of analyte solution consisting 50 mM Re(Eth) dissolved certain amount of cholesterol (1, 100, 200, 250, 300, 400, 500 μg/mL, 1, 2.5, 5, 7.5 mg/mL) was applied onto the dried $AgNO_3$ spot. Subsequently all the samples were dried in darkness for 16 h at room temperature before being detected by UV-vis spectroscopy. Reference group was

prepared with the addition of 30 μL of 50 mM Re(Eth). Duplicate samples were prepared for this part of the experiments.

2.2.6 UV-vis spectroscopy

UV-vis absorption spectra of samples obtained from each experiment, as introduced before, were recorded by Lambda 950 UV/VIS spectrometer (USA). Importantly, all the UV-vis absorption measurements focused on the up surfaces of the reaction areas, from where the solutions were added.

2.2.7 Scanning electron microscope (SEM)

EVO HD 15 (model), Zeiss (manufacturer), with LaB6 emitter, acceleration voltage 1 kV, vacuum 10^{-4} Pa, Secondary electron (SE2) detector, working distance (WD) 5~6 mm. Briefly, the cut pieces of chromatography paper spot containing the AgNP after above mentioned experiments was secured on sample stage using a double sided tape. The sample stage was inserted in its place in SEM instrument followed by switching on the vacuum pump to lower the pressure in the sample chamber. Once the pressure was below 10^{-4} Pa, the electron emitting filament was warmed up to 34°C followed by turning on the high tension to 120 kV. The sample height was adjusted such that the working distance was 5~6 mm. After setting the acceleration voltage (1 kV) for the SE2 detector and using these parameters the imaging was performed on the paper samples without any conductive coating. Once the images were recorded, the size of AgNP was quantified manually with the aid of Photoshop program. Histograms of size distribution of AgNP on paper samples in presence of various analytes were plotted using Origin 9.0, which was used to obtain values of skewness and kurtosis.

3 RESULTS AND DISCUSSION

3.1 AgNP Nucleation Controlling Ability of Paper

Based on previously published studies (Lokanathan et al., 2014; Uddin et al., 2014), it is known that the interaction between silver ion and cellulosic hydroxyl is chiefly responsible for the nucleation controlling ability of cellulose. Even though this nucleation controlling phenomenon was demonstrated for cellulose nanocrystals (CNC), it is quite logical to hypothesize that larger cellulosic materials including cellulose nanofibers (CNF) and even paper can act as nucleation controllers. The validity of this hypothesis stems from the fact that the aforementioned cellulosic materials have polymeric cellobiose or, in other words, cellulose as major constituent. A direct translation of this hypothesis is that the order in which silver ion and reducing agent introduced onto the cellulosic system would drastically affect the efficiency of silver ion reduction followed by subsequent AgNP formation. In other words, when silver ions addition precedes the reducing agent addition, the silver ions react with reducing agent without the aid of cellulosic hydroxyls. In the later scenario, one can expect poor reduction of silver ions to metallic silver species, due to the lack of assistance in nucleation by cellulosic hydroxyls. Thus, a convenient way to check if larger cellulosic materials can act as a nucleation controller would be to study the effect of the order in which silver ions and reducing agent are introduced onto the cellulosic material. In this thesis work, chromatography paper was chosen as the cellulosic material.

In order to verify the nucleation controlling ability of chromatography paper, experiments were carried out with varied amounts of reducing agent (ascorbic acid) and silver nitrate on modules where the order of layers was altered. As described in the experimental section, the module, in which the topmost layer has reducing agent while the bottom layer has silver ions, is denoted as *Re(**t**)Ag(**b**)*, while the module with opposite order is denoted as *Re(**b**)Ag(**t**)*, where "***t***" and "***b***" stand for "top" and "bottom", respectively. Once the experiments were carried out, the ***b*** layers of the

modules were analysed using UV-vis spectroscopy and the results of spectroscopic measurements are presented in figure 3.1.1.

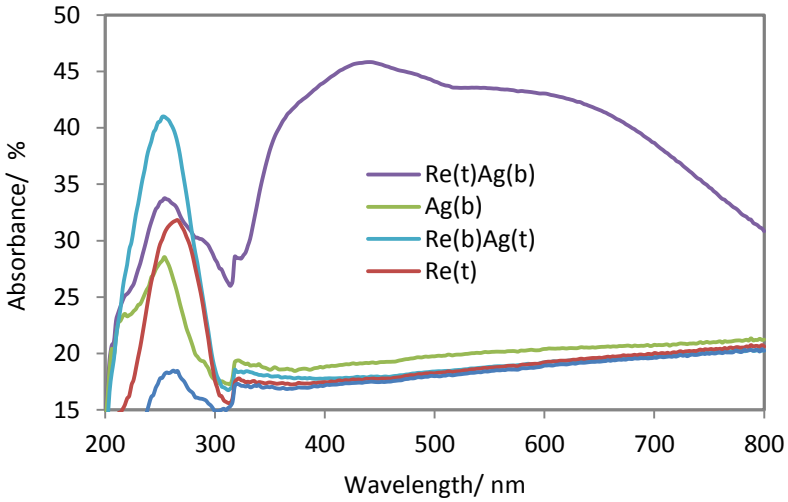

*Figure 3.1.1. UV-vis absorption spectra of sensor modules with varied sensor components. "**t**" and "**b**" stand for "top" and "bottom" layers, respectively. For instance, Re(**t**)Ag(**b**) refers to the module carrying dried 10 µL of 10 mM ascorbic acid on top layer and 10 µL of 1 mM silver nitrate on bottom layer, whereas "reference" has nothing but chromatography paper.*

As discussed in the introduction section, the presence of silver nanoparticles will result in photonic absorption corresponding to plasmonic transitions in the wavelength region of 350~800 nm. It is clear from UV-vis absorption spectra in figure 3.1.1 that none of the modules except for *Re(**t**)Ag(**b**)* presented plasmonic absorption. This observation confirmed the required module layer order in *Re(**t**)Ag(**b**)*. It is worth mentioning that in the case of *Re(**b**)Ag(**t**)*, the lack of AgNP formation could be due to the non-availability of Ag ions at the bottom layer as a consequence of the diminished diffusion or transfer of Ag ions from the topmost layer to the bottom one. Based on XPS elemental analysis (data not shown) the presence of Ag ions on the bottom layer in case of *Re(**b**)Ag(**t**)* was verified, confirming the lack of AgNP formation was due to inefficient reduction rather than

diminished migration of Ag ions. Once silver ions were added onto the ***t*** layer, though they can be carried to the ***b*** layer by later added analyte solution (just MQ water at this stage), it is most likely that the interaction between silver ions and cellulosic hydroxyls will be diminished due to the presence of reducing agent molecules. Besides, ascorbic acid has weak reduction ability, leaving no possible decrease in the energy barrier for AgNP formation. These results highlight the pivotal role of hydroxyl groups on cellulose surfaces in AgNP formation through nucleation controlling and/or stabilizing properties. Peaks of silver ions should be observed in the range of 200~300 nm (Pierre et al., 1997); however, other peaks overlap with the silver ion peak, which therefore cannot be quantitatively interpreted. For this reason, UV-vis spectra presented in later experiments will be plotted for wavelengths > 300 nm.

As discussed in the background section, any analyte that is capable of interfering with silver ion–cellulosic hydroxyl interaction would affect the nucleation and growth of AgNP during the nanoparticles forming process, thus altering the size/shape distribution of AgNP subsequently formed. A quantitative relationship between analyte concentration and the size/shape distribution of AgNP would result in a quantitative shift in plasmonic properties of resulting nanoparticles and thus form the basis of a sensor. In this thesis UV-vis absorption shall be the main analysis tool used for probing the effect of analyte on the AgNP size distribution in a quantitative manner and in future the UV-vis absorption could be the sensing signal. In order to verify the above mentioned sensing implication, representative serum biomolecules were selected. The results of corresponding studies are discussed in the following sections.

3.2 Response to Proteins

Based on the proved feasibility of *Re(**t**)Ag(**b**)* module in 3.1 section, the validity of hypothesis 2 can be tested. The operation of the sensor module-*Re(**t**)Ag(**b**)* in presence of the two most abundant mammalian proteins (BSA, γ-globulin) is

discussed. The isoelectric points of BSA and γ-globulin are 4.7 (Ge et al., 1998) and 6.5 (Cann et al., 1949), respectively, in water at room temperature (pH value of MQ water is 8.5 at room temperature). Thus, both BSA and γ-globulin are anionic upon denaturation during the AgNP forming process. Since the sensor is targeted at biosensing applications pertaining to human blood, the working concentrations of BSA and γ-globulin were chosen based on the normal levels of human serum albumin and γ-globulin, as introduced in methodology section. Both lower and higher concentrations that are out of the normal concentration ranges were chosen to represent unhealthy conditions. The results of corresponding UV-vis absorption studies are presented in figure 3.2.1.

As it is shown in figure 3.2.1, the entire UV-vis absorption spectra display plasmonic peaks within the wavelength range for all samples. In the case of BSA, both peak positions at short and long λ_{max} are constant at 434 and 538 nm, respectively. Besides, both plasmon peak intensity variations are quite limited, as it is seen in figure 3.2.1(a). If changes in the plasmonic peak position or intensity is to be used, the presented absorption spectra suggest that the current *Re(**t**)Ag(**b**)* sensor is not sensitive to BSA. Nevertheless, a noticeable plasmon band intensity variation of γ-globulin samples can be observed (figure 3.2.1(b)). However, this does not indicate a sensitive sensor to γ-globulin, since the variation of plasmon band does not follow expected trends. Based on the introduction of plasmon peak variation, subsequently enhanced peak intensity at short λ_{max} is expected, when there is a peak intensity decrease at long λ_{max}. However, contrary to expectation, peak intensity decrease happens at the same pace within the whole wavelength range over all samples. Thus, one can speculate that there might be some impurities, like salts, that consume the redox reaction components, interfering AgNP formation. For instance, a direct consequence of the presence of salt impurities would be the preferred precipitations of silver salts, like AgCl, leaving less silver ions to react with ascorbic acid. Therefore, in order to check the influence of salts on AgNP forming process, experiments with KHB minerals salts were carried out. Corresponding UV-vis absorption spectra are presented in figure 3.2.2.

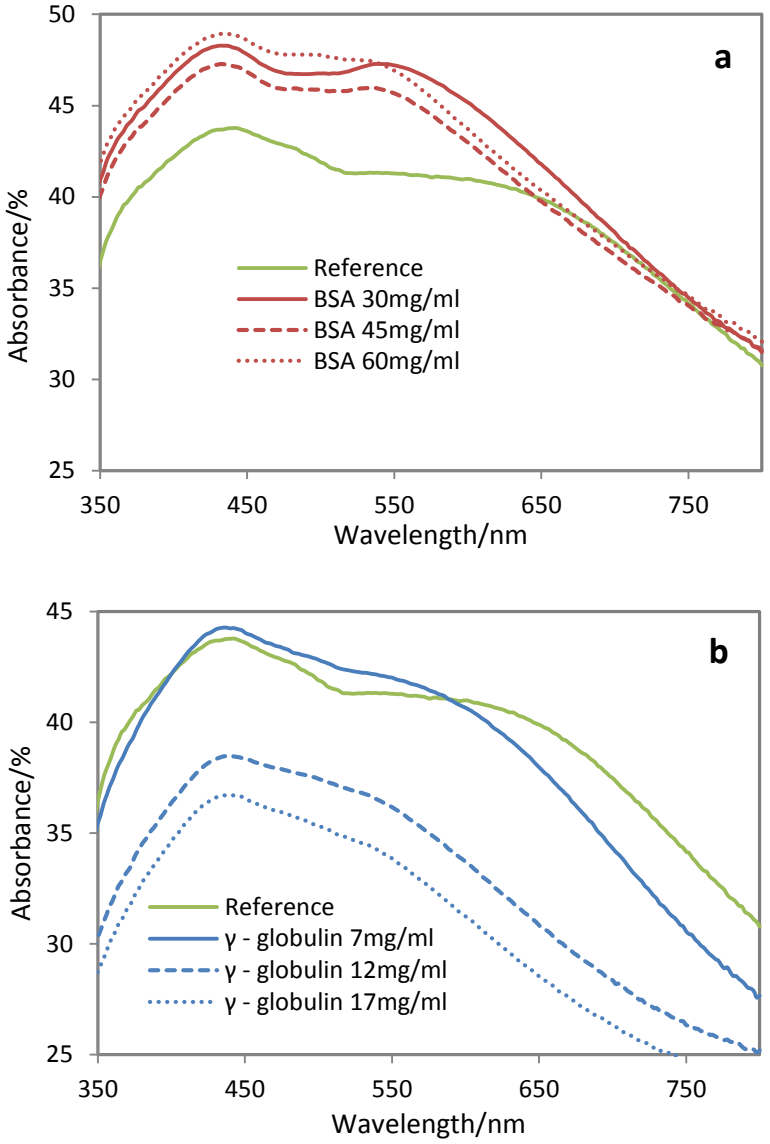

*Figure 3.2.1. UV-vis absorption spectra of AgNP formed in presence of given amounts of proteins in the Re(**t**)Ag(**b**) sensor module: (a) BSA; (b) γ-globulin. Reference samples represent the AgNP formed with MQ water alone.*

It is clear from figure 3.2.2 that KHB salts can affect the formed AgNP at different levels, raising the possibility of salts as interfering substances. With regard to the actual human internal environment, the presence of NaCl as a main electrolyte component significantly limited the sensor by consuming the silver ions due to AgCl precipitation. Regardless of the detailed variations in the formed AgNP in

presence of each salt concentration, it is still noticeable that the least influence on formed AgNP happens at the lowest concentration of each salt. This suggests a possible application condition for the current sensor system, that is, to dilute 10-fold the original analyte solution before its addition onto the sensor module. However, the properties of the analyte should be taken into consideration for the current module to be able to respond to the analyte concentration effectively. In other words, the dilution of analyte can only make sense when the sensor module is capable of supporting distinct absorption spectra of the formed AgNP in presence of diluted proteins. In this case, it could be of importance to carry out control experiments by synthesizing AgNP on sensor modules in presence of purified (i.e. through dialysis) proteins with certain concentration gradients, as well as by substituting KHB buffer for MQ water as the solvent in the last control experiment.

In addition, from the ion charge point of view, the KHB salts could be classified into two groups: mono-charged and bi-charged. However, since experiments were carried our based on the KHB salts content, the effect of ions would be difficult to analyse due to their different concentrations in molar units.

To summarize, further experiments with purified proteins should be helpful to gain more understanding of the AgNP forming mechanism on *Re(**t**)Ag(**b**)* module in presence of proteins. Simplified studies with model analytes may facilitate the study of sensor for proteins. Therefore, ionic and nonionic surfactants were selected for such tests. The results of proof of concept studies using these model systems is discussed in the following section.

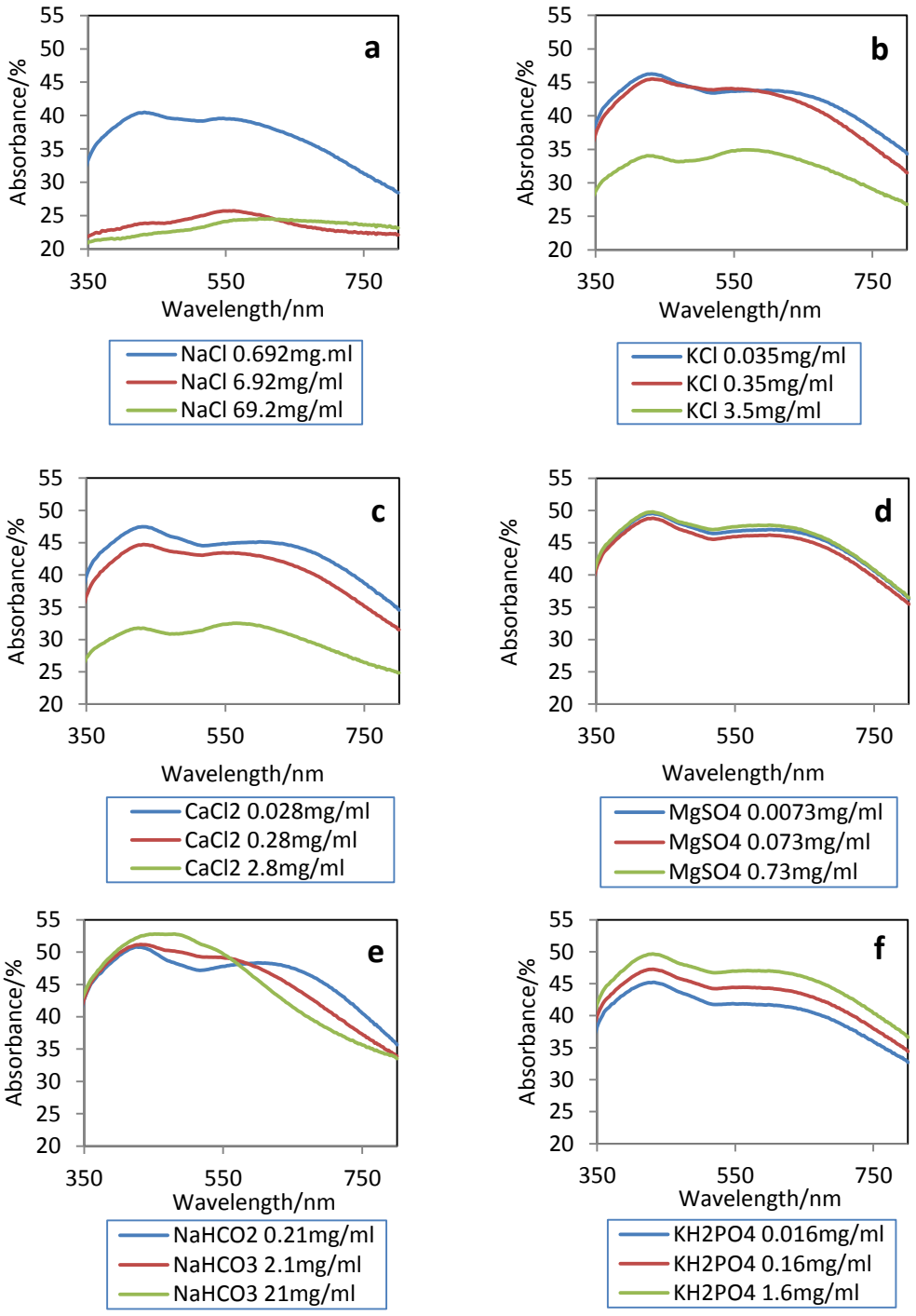

*Figure 3.2.2. UV-vis absorption spectra of AgNP formed in presence of KHB salts of varied concentrations on the sensor module of Re(**t**)Ag(**b**): (a) NaCl; (b)KCl; (c) $CaCl_2$; (d)$MgSO_4$; (e) $NaHCO_3$; (f) KH_2PO_4. Where, red lines represent the concentrations of KHB salts.*

3.3 Response to Surfactants

Given that the module idea for AgNP formation has been standardized by the studies in above sections, it is clear that the factors that influence the AgNP formation would be the affinity competitions among Ag(0), Ag^+, Re, and hydroxyl groups on cellulose surfaces. Surfactants, including cationic, anionic, and nonionic species, shall be promising candidates not only to study these affinity changes which may affect AgNP formation, but also to mimic potential analyte biomolecules in real applications.

In an attempt to demonstrate the sensing potential of *Re(**t**)Ag(**b**)* module, cationic (DDAB), anionic (SDS), and nonionic (Triton X) surfactants were chosen. The *Re(**t**)Ag(**b**)* module was modified as described in the methodology section. In short, a fixed volume of solution of surfactant and reducing agent was added onto a spot on chromatography paper bearing silver ions. The molecular size and shape of specific surfactant molecules chosen are comparable. In essence, among these surfactants the main variant is the hydrophilic polar head group. By choosing the working concentrations of surfactants to be below cmc values, it can be safely assumed that the observed results were due to the effect of individual analyte (surfactant) molecule behaviour, rather than due to their self-assemblies. Hence by working below cmc, the interpretation of observed plasmonic properties might be less complicated.

In order to check the influence of surfactants below cmc, a wide range of submicellar concentrations were studied. The results of UV-vis absorption studies performed on paper surfaces with AgNP synthesized in presence of three different surfactants are presented in figure 3.3.1.

It is clear shown that all absorption spectra exhibit two characteristic plasmonic peaks (~420 nm; 500~600 nm). In order to make the differences in the plasmonic region visually more apparent, three more spectral data sets with narrowed

wavelength range are included in figure 3.3.1(b, c, d). The position of the individual plasmon peak along with the intensity was used to compare the size and shape distribution of AgNP formed in these experiments. The shift in intensity at short (~420 nm) and long (500~600 nm) wavelength plasmon peaks for the various surfactants are presented in figure 3.3.2. Additionally, the plasmon peak positons of λ_{max} in long wavelength range (500~600 nm) are also presented in figure 3.3.2. Since there were no significant changes in plasmon peak positons of λ_{max} in short wavelength range (~420 nm) across three surfactants samples species, these values have not been included.

As discussed in introduction section, the peak intensity is related to the number of nanoparticles, while the position is related to the size and shape of the plasmonic nanoparticles. It can be seen from figure 3.3.2 that "blue shifts" of long wavelength plasmon peaks occur in the presence of all surfactants samples as a function of increasing concentration. This suggests a decrease in AgNP size. It is known that the long λ_{max} peak is due to the presence of larger AgNP (non-spherical), which were formed due to the growth of smaller silver particles. Thus, as a consequence, a blue shift of long λ_{max} plasmon peak is expected to increase the number of smaller AgNP, which would result in the plasmon absorbance of λ_{max} at short wavelength region (~420 nm). This expectation can be clearly verified from the intensity values presented in figure 3.3.2, showing that the intensity at short λ_{max} peak rises with increasing concentration of surfactant. This increase in intensity is due to the raise in number of AgNP alone, rather than the increase in AgNP size, which could also result in the intensity enhancement. The exclusion of the possibility of AgNP size as a contributor to the increased peak intensity is based on the fact that, no corresponding red shift was observed, which should be expected if the size of plasmonic particles were to grow.

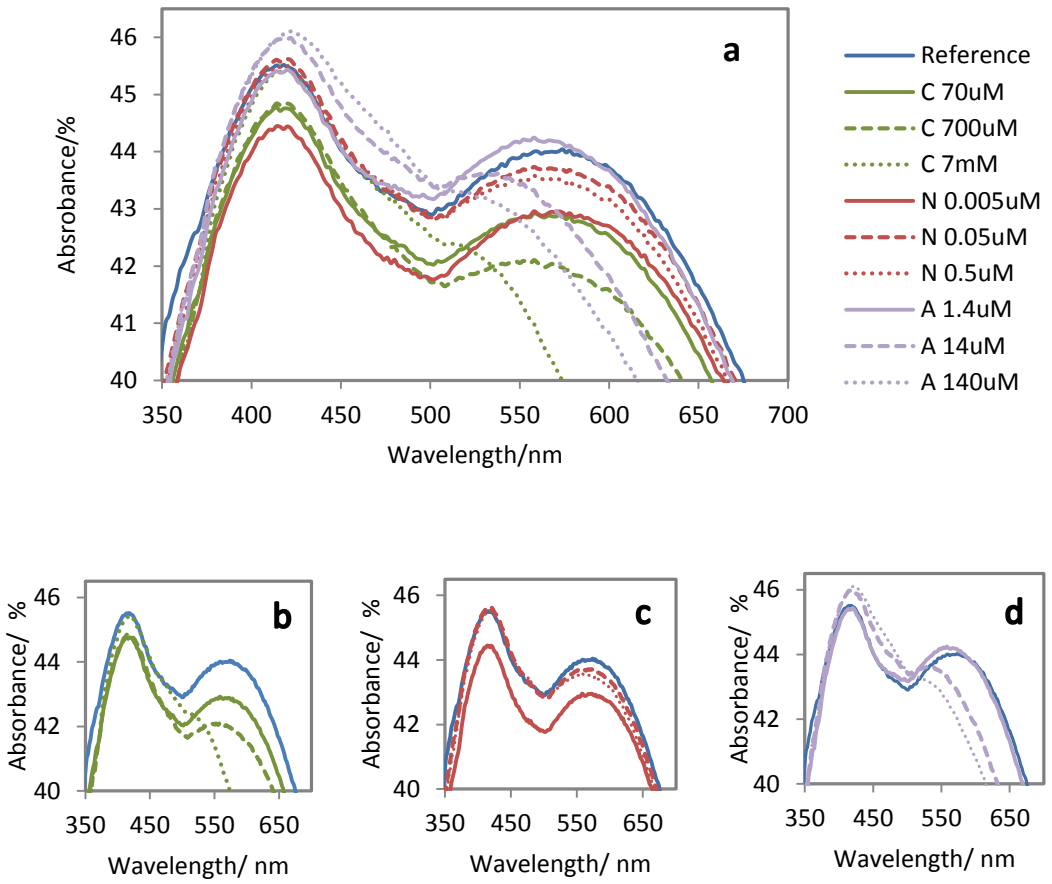

Figure 3.3.1. (a) UV-vis absorption spectra of AgNP formed in presence of surfactants whose concentrations were kept below the cmc: (b) cationic surfactant ("C")-DDAB; (c) nonionic surfactant ("N")-Triton X-100; (d) anionic surfactant ("A")–SDS.

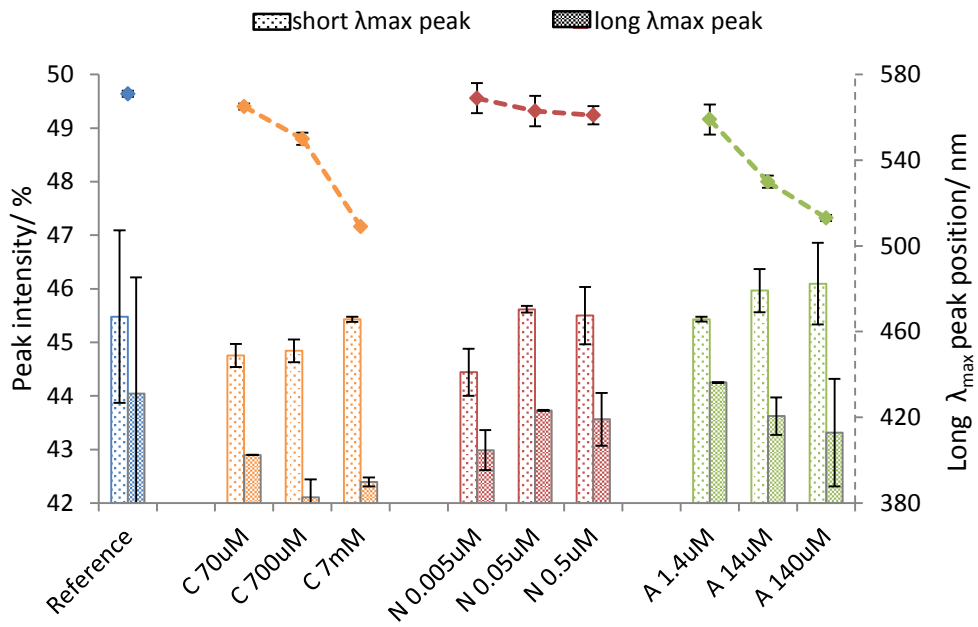

Figure 3.3.2. Characterization of plasmon peaks of AgNP formed in presence of surfactants. Peak intensities and shifts at λ_{max} were shown in columns and dash lines, respectively. Where, "C", "N", "A" stand for "cationic", "nonionic" and "anionic" surfactants, respectively.

Apart from general trends in peak position and intensity as a function of surfactant concentration, very interesting results can be observed by interpreting the spectral data as a function of the charge of analyte molecules. Surface of AgNP upon formation can develop a partial negative charge due to the absorption of oxygen followed by oxidation of the surface (Ilknur et al., 2012). For such a partially negatively charged AgNP surface, one can expect that, among the surfactants under consideration, cationic surfactant (DDAB) molecules have the highest affinity for AgNP surface, followed by nonionic ones (Triton X), whereas anionic species (SDS) have the lowest affinity. Upon comparison, it becomes clear that cationic surfactant causes much higher blue shift of the long wavelength plasmon peak relative to anionic and nonionic surfactants. Considering the fact that, in spite of the higher affinity of cationic surfactant towards cellulose surfaces, the cationic surfactant also has higher affinity for metallic silver surfaces. Therefore, the most probable reason

for the relatively higher blue shit in the case of cationic surfactant could be explained by the enhanced passivation of AgNP growth through absorption of cationic head groups on metallic silver surfaces, thereby preventing the formation of larger non-spherical AgNP. In addition, an alternate explanation is worth considering, which is with regard to the fact that the electrostatic anionic nature of paper arises from non-cellulosic molecules such as hemicellulose. Upon addition of the cationic surfactant, its cationic head groups can bind to the anionic groups on paper through Columbic interaction, while the hydrophobic tails are exposed at the interfaces. Hence, the water wettability of anionically charged areas on paper diminishes due to the presence of hydrophobic tails of surfactant molecules. A direct consequence of diminished wettability of anionic areas would be the increased aqueous availability near cellulosic hydroxyls rich regions of paper, and such an effect could enhance the rate of reduction because of the larger influx of reducing agent, leading to a faster nucleation subsequently. This faster nucleation would compete with the growth of silver particles, thereby lowering the number of larger AgNP, and increasing the number of smaller AgNP. The chief distinction between the first mentioned AgNP surfaces passivation explanation and the latter proposed nucleation enhancement theory is that, in the case of the former discussion, the observed effect is due to the interaction between silver metallic surface and cationic surfactant. Nevertheless, in the case of latter discussion, the blue shift observed is because of the interaction between anionic surface of paper and cationic surface of surfactant. To figure out the essential mechanism behind the blue shift caused by cationic surfactant, more detailed experiments will be needed in future studies.

Results of anionic and nonionic surfactants are quite surprising if AgNP surface passivation theory is to be considered, namely, nonionic surfactant should cause larger blue shift than anionic species, based on the fact that there will be electrostatic repulsion between anionic head groups of anionic surfactant and negatively charged surfaces of silver particles as well as paper surface. Results contradicting this expectation can be observed in figure 3.3.2. One of the possible explanations for these phenomena could be supported from previous studies (Uddin

et al., 2014), indicating that, in the case of CNC, the surface hydroxyls are responsible for nucleation controlling ability and the anionic groups are responsible for stabilizing the AgNP. Therefore, the final AgNP size distribution depends on both nucleation rate and the growth rate. Upon nucleation of AgNP, silver particles continue to grow in size and gradually develop a negative charge due to oxygen absorption. Anionic groups are capable of stabilizing non-oxidized AgNP by donating electron density to metallic surfaces. As a consequence, anionic surfactant molecules are capable of stabilizing AgNP immediately after their formation before they develop negative charges. This superior stabilizing capability of anionic surfactant would result in a lower growth rate and thus hinder the formation of larger AgNP, which contribute to the plasmonic absorbance in long wavelength range (500~600 nm), as well as the blue shift in that wavelength region, which is what was observed experimentally.

In addition to the proposed explanations with regard to the surfactant-AgNP interaction, it is also worth considering the surfactant-cellulose interaction. It is known that both anionic and nonionic surfactants absorb on hydrophobic regions of amphiphilic cellulose. Cellulose surfaces have both hydrophobic and hydrophilic sites adjacent to each other. During the AgNP formation in presence of anionic surfactant, the nucleation happens on the hydrophilic sites (hydroxyl rich) and maybe subsequently stabilized by anionic head groups from surfactant absorbed on neighbouring hydrophobic sites. Hence, the interaction of cellulose with anionic surfactant could add a proximity advantage which enables superior stabilizations of AgNP immediately after their formation. This significant proximity contribution becomes apparent upon a closer look at the control samples, without surfactants. Surface anionic groups on paper may not necessarily be homogenously distributed proximal the cellulosic hydroxyls rich regions on paper, due to the presence of non-cellulosic molecules. Thus, AgNP which is nucleated on the cellulosic hydroxyls rich regions may not be stabilized immediately as they migrate around until the final stabilization. Results in figure 3.3.2 agree with the latter explanation, showing a higher intensity value at long wavelength plasmon peak (~44%) of reference group, when compared to that of anionic surfactant presented samples (~43%) at their

highest concentrations. Effects of surfactants on size distribution cannot be directly analysed with UV-vis spectroscopy alone. The results of these optical studies shall be consolidated by complementary studies such as direct visualization of AgNP. In this thesis work, SEM was used to learn the exact size distribution of AgNP formed on paper. Corresponding results from SEM based characterization will be presented in the following sections.

In order to exclude the effect of concentration and thus obtain a preliminary idea of the effect of charge on surfactants` head groups on the same level, AgNP synthesis experiments were carried out in presence of 140 μM surfactants for all species. Representative SEM images of AgNP on paper surfaces synthesized in presence of three different surfactants are presented in figure 3.3.3. Their corresponding histograms are presented in figure 3.3.4. Since SEM images themselves do not provide any direct quantitative information about AgNP, detailed statistical parameters (mean diameter, skewness and kurtosis values) of AgNP size distribution obtained from histograms and listed in table 3.3.1 were used to understand the mechanisms. Upon comparing the skewness and kurtosis values, the four AgNP samples species can be grouped into two. The cationic and anionic surfactants samples have skewness values within the range (-1, +1), indicating these samples have non-skewed, symmetrical size distribution, thereby hinting minimal aggregations relative to nonionic and reference samples, of which both have positive skewness values above +1. Moreover, these higher positive values of nonionic and reference samples imply significant aggregations. Additional information on how narrow the AgNP size distribution is can be inferred from kurtosis values. Therein, ionic samples have kurtosis values within the range (-1, +1), representing a much narrower size distribution compared to nonionic and reference samples, of which kurtosis values are 2.2 and 1.5, respectively. It is interesting to correlate the size distribution related conclusions derived from UV-vis absorbance studies with that obtained from SEM analysis. The narrower and symmetrical size distributions in terms of ionic surfactants presented samples support the UV-vis observations, from which these surfactants resulted in larger blue shifts relative to the other two sample species. Thus, it is possible to conclude

that the nucleation and growth of AgNP were better controlled in samples with ionic surfactants compared to nonionic and reference samples.

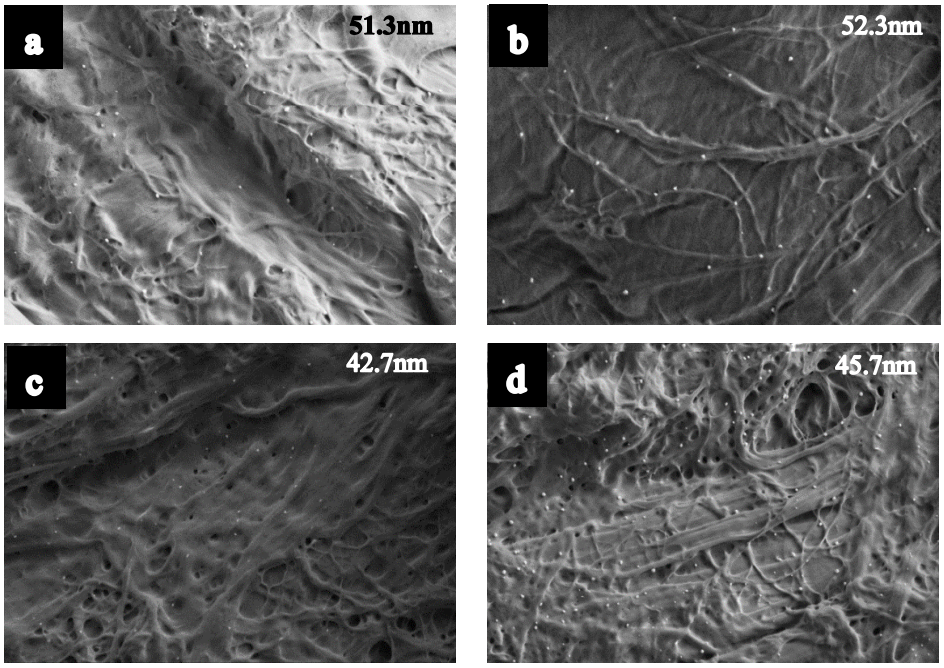

Figure 3.3.3. SEM images of AgNP formed on paper in presence of no surfactants (a); cationic surfactant-DDAB (b); nonionic surfactant-Trition X-100 (c); anionic surfactant-SDS (d). Mean size of AgNP is shown in each panel. Scale bars applied in SEM images are all 1 μm.

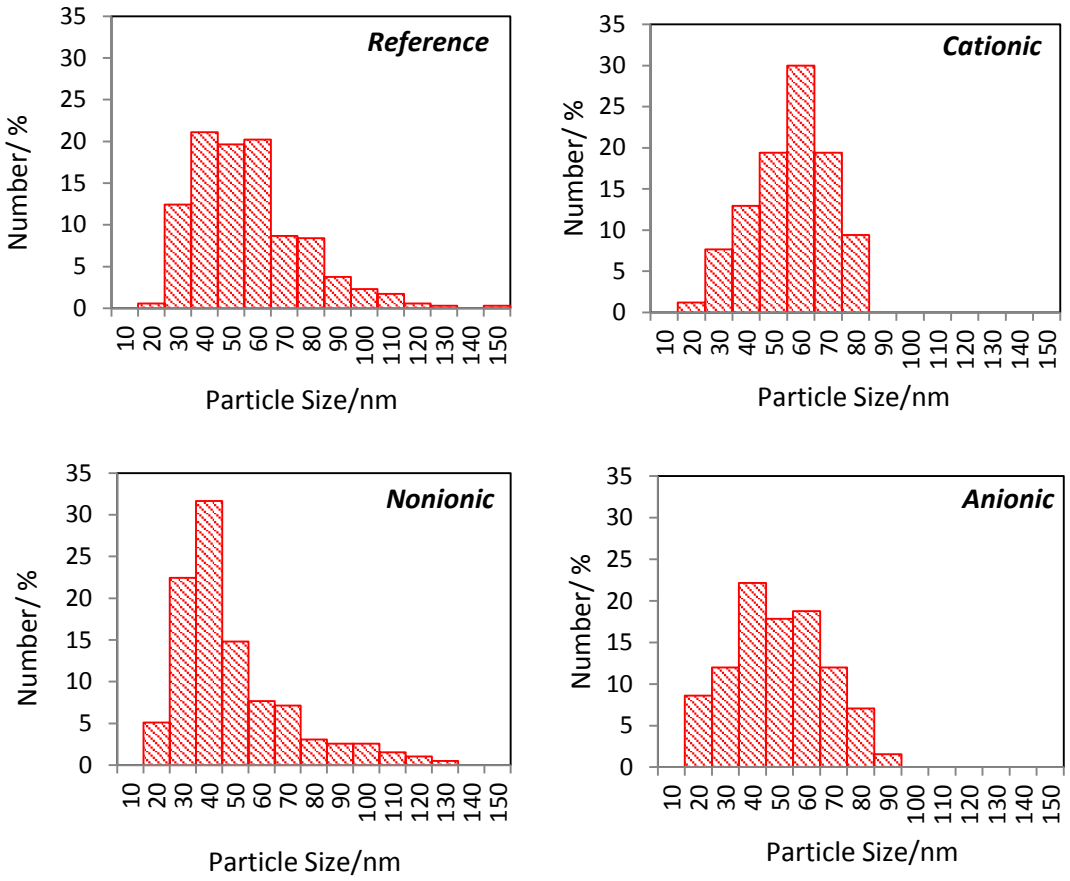

Figure 3.3.4. AgNP size distributions of corresponding SEM images in figure 3.3.3.

Table 3.3.1. Statistical Parameters of corresponding histograms of AgNP size distribution in figure 3.3.4.

	Mean Size/nm	**Skewness**	**Kurtosis**
Reference	51.3±20.2	1.1	1.5
Anionic	45.6±17.2	0.2	-0.6
Cationic	52.3±14.3	-0.3	0.5
Nonionic	42.7±21.3	1.5	2.2

3.4 Response to Cholesterol

Provided that surfactants can effectively influence the formation of AgNP on paper, it shall be interesting to explore more about this model system with biomolecules. In this case, cholesterol was chosen for this part of experiments. As described in the experimental section, experiments in presence of cholesterol were carried out basically in the same way as that of experiments in presence of surfactants. However, the solvent for ascorbic acid and cholesterol was ethanol instead of MQ water. Additionally, according to the implications of varied cholesterol levels over a broad range (Ockene et al., 2004), working concentrations of cholesterol were planned to cover the highest concentration. According to the dissolution condition described in experimental section, preliminary experiments suggested 7.5 mg/mL cholesterol to be the highest concentration available. Thus, primary tests with cholesterol were planned to focus on the concentration range of 1 μg/mL~7.5 mg/mL. Corresponding UV-vis absorbance spectra are presented in figure 3.4.1.

As can been from figure 3.4.1, UV-vis absorption spectra of AgNP formed in presence of varied amounts of cholesterol appear to have similar characteristic plasmonic peaks to those in figure 3.3.1, namely, one at ~430 nm and the other one in the long wavelength range of 500~750 nm, representing the formation of small AgNP and aggregated AgNP, respectively. The plasmonic peak positions in the long wavelength region across all samples, as well as plasmonic peak intensities of all samples in both short and long wavelength regions are included in figure 3.4.2. As before, these plasmonic peak positions at short λ_{max} over all concentrations were not included because the negligible variations at ~430 nm.

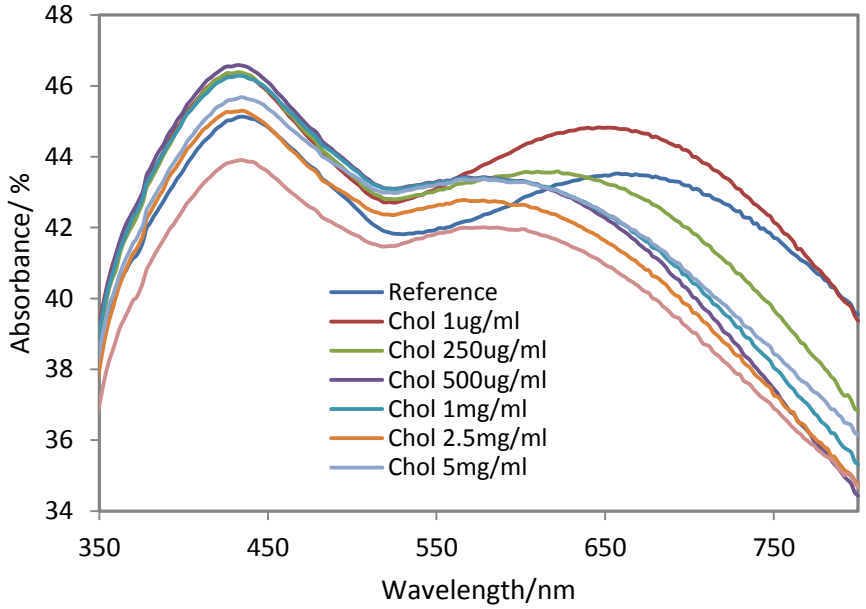

Figure 3.4.1. UV-vis absorption spectra of AgNP formed in presence of varied amounts of cholesterol (0~7.5 mg/mL). Where "Chol" stands for "cholesterol".

From figure 3.4.2(a) it is clear that the plasmonic peak positons of long λ_{max} peaks decrease in presence of cholesterol as a function of increasing concentration. Specifically, a distinct blue shift throughout long λ_{max} peaks can be observed within the cholesterol concentration range of 1~500 µg/mL, indicating a controlled growth of smaller AgNP. Considering the fact that plasmonic peak intensity is affected by both the number and the size of plasmonic particles, thus, controlled particle growth should correspondingly lead to an increased amount of smaller AgNP. Therefore, one can expect either a decrease in long λ_{max} peak intensity, or an increase in short λ_{max} peaks intensity, compared to reference group. With regard to the first possibility, it is verified by the general trend in the peak intensities at long λ_{max}. Additionally, the second expectation can be confirmed by the increased short λ_{max} peak intensity, as it is shown in figure 3.4.2(a). The relatively flat trend in both the long λ_{max} peak position and intensity could possibility result from the self-assemblies of cholesterol, which may affect the AgNP formation mainly by steric hindrance, apart from working as a nucleation controller via AgNP-cholesterol and cellulose-cholesterol interactions.

Based on the observation that a distinct blue shift of long λ_{max} peak occurs in presence of cholesterol within the range of 0~500 μg/mL, it would be interesting to investigate how sensitive the sensor system can respond to varied amounts of cholesterol within that effective working concentration range. The ideal correlation between cholesterol`s concentration and the long λ_{max} peak position should be a linear trend, which might be an important quality for a good sensor. Thus, in order to investigate this idea, the same experiments with narrowed concentration intervals were carried out, and the relevant analysis of plasmonic peaks are included in figure 3.4.2(b). As can be seen, the general trend of both plasmonic peak position and intensity are consistent with those in figure 3.4.2(a) within the same concentration range of cholesterol. Nevertheless, no linear changes in blue shift can be observed, nor regular trend in plasmonic peak intensities. These observations imply the poor sensitivity of the present sensor system. Moreover, compared to the results of samples in presence of 1 μg/mL cholesterol in figure 3.4.2(a), unexpected results are observed in figure 3.4.2(b). As the paper substrates used in this thesis were directly used without any pre-purification treatment, this unexpected increase might be due to the presence of impurities on the paper surface, which may occupy the effective nucleation controlling sites. In addition to the poor sensitivity performance of the current sensor system, there was a lack of repeatability.

In spite of above mentioned poor performances as a sensor, it is still of interest to explore the essential mechanism of AgNP formation in presence of cholesterol. As it is shown in figure 3.4.2(b), regardless of the fluctuations over the trends in long λ_{max} peak position and intensity, nucleation controllability of cholesterol can be established by the general descending trend in long λ_{max} peak positions and by the overall enhancement in short λ_{max} peak intensities, indicating a decrease in lager AgNP size and an increase of smaller AgNP number, respectively. With the purpose to get a more clear understanding of AgNP size distribution, SEM studies of the reference group (without cholesterol) and sample group in presence of 300 μg/mL cholesterol, were carried out. The reason for choosing 300 μg/mL cholesterol, instead of 500 μg/mL cholesterol, is that there is a lack of an apparent blue shift over long λ_{max} peaks. Besides, it could be of importance to investigate how the

AgNP formation can be significantly affected by the presence of cholesterol within the most effective working concentrations at the initial point. Thus, representative SEM images of non-cholesterol and 300 μg/mL samples are presented in figure 3.4.4(a, b). In addition, their corresponding histograms, as well as the relevant statistical parameters (skewness and kurtosis), are also included in figure 3.4.4(c).

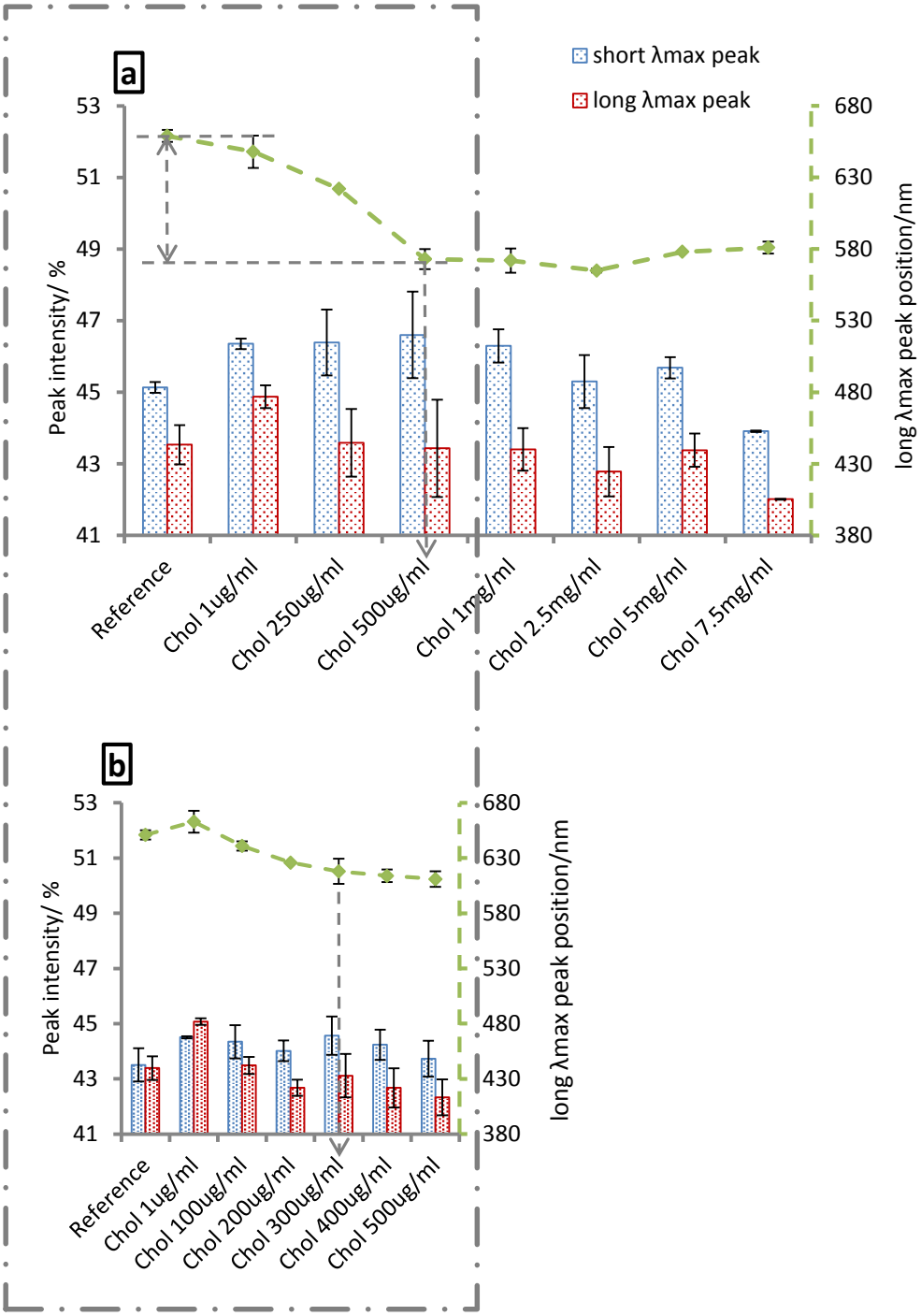

Figure 3.4.2. Characterization of plasmonic peaks of AgNP formed in presence of cholesterol over a concentration range of (a) 0~7.5 mg/mL; (b) 0~500 µg/mL. Peak intensities and shifts at λ_{max} are shown in columns and dash lines, respectively.

According to the proposed reasons explaining surfactants function as a nucleation controller and stabilizer, the mechanism of cholesterol to affect AgNP formation could also be explained from two perspectives.

On one hand, upon absorbing cholesterol onto paper surface, the exposed polar/nonpolar tails of cholesterol can either influence the formation of AgNP assemblies by steric hindrance, or help fasten the stabilization of AgNP via polar-silver interactions. In either case, an improved nucleation and stabilization of subsequently formed AgNP were expected, which should be followed by a narrowed particle size distribution, concentrating on a range of smaller particle sizes. This speculation can be checked by the results displayed in figure 3.4.4. Compared to reference group (kurtosis=-0.3, skewness=0.4), cholesterol (300 μg/mL) group has a higher kurtosis value at 5.0 and higher skewness values at 1.5. As it is known that lower the absolute value of skewness, the more symmetric is the size distribution. The lower the absolute value of kurtosis, the closer the histogram is to a normal distribution. With a higher positive kurtosis value, the histogram will tend to have a distinct peak near the mean value, and accompanied by "tails" on two sides with rapid decline. A higher positive skewness value represents a more concentrated distribution in lower range values. In the case of cholesterol (300 μg/mL) group, size distribution is more peaked and closes to a smaller mean size (40.8±14.8 nm), confirming the controlled nucleation of AgNP. However, its asymmetric size distribution may indicate poor stabilization ability. Whereas, this does not imply 300 μg/mL cholesterol led to much more severe aggregations of AgNP compared to reference group. Otherwise, a red shift, rather than a blue shift in figure 3.4.2, should be observed in the general trend of long λ_{max} peak positions in UV-vis spectra over all sample species. Nevertheless, this high skewness value does suggest cholesterol to have a limited stabilizing capability of AgNP, compared to its noticeable ability to influence nucleation through its interaction with paper surface.

On the other hand, cholesterol may donate electron density to partially negatively charge silver particles surfaces, increasing the Fermi level subsequently. Therefore,

as a consequence, the growth of smaller metallic silver particles was hindered, in other words, AgNP can be faster stabilized in the presence of cholesterol. Thus, as a result, there will be an increase in the number of smaller AgNP, which could lower the average particle size of samples with 300 µg/mL cholesterol compared to those without cholesterol. This is consistent with the mean particle size results presented in figure 3.4.4(a, b). However, taking into account of the structure of cholesterol, this supposed electron donating capacity of cholesterol can be quite small due to the presence of large dominant hydrophobic group (figure 3.4.3). Therefore, it should still be the interaction between paper and cholesterol that favours the increase in smaller particle number.

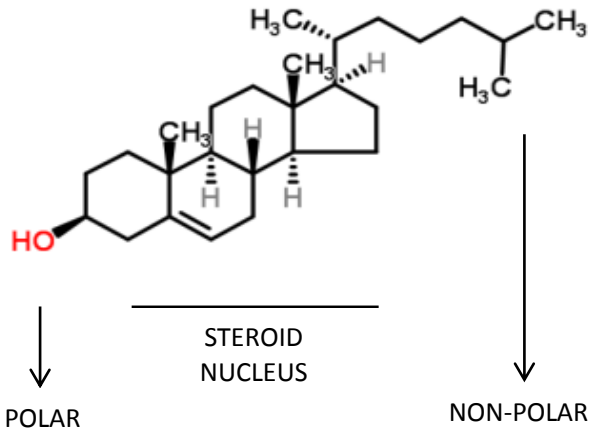

Figure 3.4.3. Structure of a cholesterol molecule.

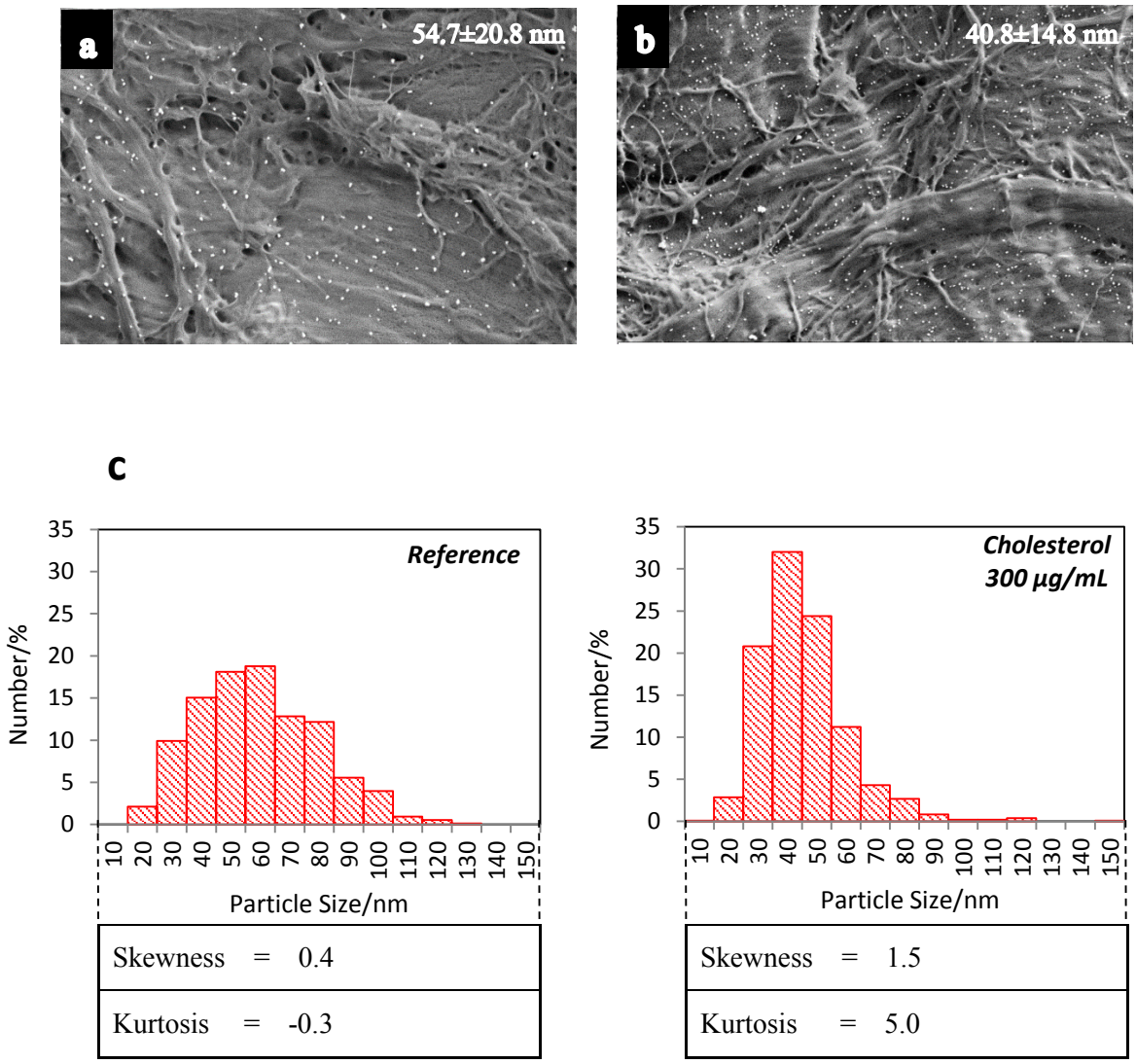

Figure 3.4.4. SEM images of AgNP formed on paper in presence of non-cholesterol as reference (a) and of 300 µg/mL cholesterol (b). Corresponding histograms and their statistical parameters of AgNP size distributions are presented in (c). Mean sizes of AgNP are shown in each panel of SEM images. Scale bars applied in SEM images are all 1 µm.

4 CONCLUSION

A 3-layer sensor module was built to study the capability of paper as AgNP nucleation controller. By altering the addition order of silver nitrate and ascorbic acid onto the ***t***- and ***b***- layer in module, a preferred *Re(**t**)Ag(**b**)* module was established, after confirming the essential prerequisite to form the cellulosic hydroxyl-Ag^{+} interaction. Validity of this *Re(**t**)Ag(**b**)* module was verified by plasmon band in UV-vis absorption spectra. Representative plasmonic peaks were observed at ~420 nm and within 500~600 nm wavelength region, which derived from AgNP formation. With these evidences, proposed hypothesis 2 is verified.

Studies with proteins (BSA, γ-globulin) with *Re(**t**)Ag(**b**)* module supported the hypothesis 1, namely, analyte can influence the formed AgNP. In addition, obtained UV-vis spectra of both proteins and KHB salts suggests the need of more fundamental exploration for *Re(**t**)Ag(**b**)* sensing. Besides, based on obtained results, future applications might require high levels of protein purifications, as well as dilution of analyte to magnify the sensor`s response.

The performed model system studies with surfactants (cationic, anionic, nonionic) with their distinct hydrophilic head groups verified hypothesis 1. UV-vis spectra and SEM results both indicated that the cationic surfactant (DDAB) is the most influential for AgNP formation, followed by anionic (SDS) and nonionic (Triton X) surfactants. These observations may benefit future studies with substances having corresponding features. Mechanisms behind these observed phenomena were proposed. In short, AgNP forming process can be influenced by surfactant-silver interaction, and/or by surfactant-cellulose adsorption.

A further study involved a model cholesterol system. UV-vis studies with cholesterol (0~500 μg/mL) implied the poor sensitivity and reliability of the present

sensor, which failed to quantify analyte concentrations. Nevertheless, the SEM results indicated nucleation control by cholesterol.

In conclusion, the findings in this thesis not only are consistent with previous related studies but also highlight the possibility of a sensor by intervening in the AgNP forming process, rather than by using pre-synthesized AgNP. Further exploration on the mechanisms involved will be needed to reach this goal.

REFERENCE

Adam D., McFarland, & Richard P. Van Duyne. Single silver nanoparticles as real-time optical sensors with zeptomole sensitivity. *Nano Lett.* 3(2003):8.pp. 1057–1062.

Arcot R. Lokanathan, Khan Mohammad Ahsan Uddin, Orlando J. Rojas & Janne Laine. Cellulose nanocrystal-mediated synthesis of silver nanoparticles: role of sulfate groups in nucleation phenomena. *Biomacromolecules.* 15(2014):1.pp. 373-379.

Cann John R., Brown Raymond A. & Kirkwood John G. Application of electrophoresis-convection to the fractionation of bovine γ-globulin. *J. Biol. Chem.* 181 (1949):1.pp. 161-170.

Carlos Caro, Paula M. Castillo, Rebecca Klippstein, David Pozo & Ana P. Zaderenko. Silver nanoparticles: sensing and imaging applications. chapter 11. silver nanoparticles. *InTech*. 2010. 201-225p.

Chang H. Lee, Mikella E. Hankus, Limei Tian, Paul M. Pellegrino & Srikanth Singamaneni. Highly sensitive surface enhanced raman scattering substrates based on filter paper loaded with plasmonic nanostructures. *Anal. Chem.* 83(2011):23.pp. 8953–8958.

Chen Y. & Lu C. Surface modification on silver nanoparticles for enhancing vapor selectivity of localized surface plasmon resonance sensors. *Sens. Act. B*, (2009):135.pp. 492–498.

Corti MC, Guralnik JM, Salive ME, Sorkin JD. Serum albumin level and physical disability as predictors of mortality in older persons. *JAMA.* 272(1994):13.pp. 1036-1042.

David D. Evanoff Jr. & George Chumanov. Synthesis and optical properties of silver nanoparticles and arrays. *ChemPhysChem.* 6(2005).pp. 1221 – 1231.

Feofanov AV, Grichine AI, Shitova LA, Karmakova TA, Yakubovskaya RI, Egret-Charlier M & Vigny P. Confocal raman microspectroscopy and imaging study of theraphthal in living cancer cells. *Biophys. J.* 78(2000):1.pp. 499-512.

Ge S, Kojio K, Takahara A. & Kajiyama T. Bovine serum albumin adsorption onto immobilized organotrichlorosilane surface: influence of the phase separation on protein adsorption patterns. *J. Biomater. Sci. Polym. Ed*. 9(1998):2.pp. 131-50.

Geert Cornelis, Casey DooletteMadeleine Thomas, Mike J. McLaughlin, Jason K. Kirby, Douglas G. Beak & David Chittleborough. Retention and dissolution of engineered silver nanoparticles in natural soils. *Soil Sci. Soc. Am. J*. 76(2012):3.pp. 891-902.

Gilberto Siqueira, Julien Bras & Alain Dufresne. Cellulosic bionanocomposites: a review of preparation, properties and applications. *Polymers.* 2(2010).pp. 728-765.

He Junhui, Kunitake Toyoki & Watanabe Takeshi. Porous and nonporous Ag nanostructures fabricated using cellulose fiber as a template. *Chem. Commun.* 2005, 795-796.

He Liu (a), Dan Wang, Shibin Shang, Zhanqian Song. Synthesis and characterization of Ag–Pd alloy nanoparticles/carboxylated cellulose nanocrystals nanocomposites. *Carbohydr. Polym.* 83(2011):1. pp. 38-43.

He Liu (b), Dan Wang, Zhanqian Song, Shibin Shang. Preparation of silver nanoparticles on cellulose nanocrystals and the application in electrochemical detection of DNA hybridization. *Cellulose.* 18(2011):1.pp. 67-74.

Hirano S., Wakasa Y., Saka A., Yoshizawa S., Oya-Seimiy Y.a, Hishinum Y.b, Nishimur A., Matsumoto A. & Kumakur H. Preparation of Bi-2223 bulk composed with silver-alloy wire. Physica C: *Superconductivity and its Applications* 392-396(2003):part 1.pp. 458-462.

Hong Dong , Edmond Fey , Anna Gandelman & Wayne E. Jones , Jr. Synthesis and assembly of metal nanoparticles on electrospun poly(4-vinylpyridine) fibers and poly(4-vinylpyridine) composite fibers. *Chem. Mater. 18* (**2006**):8.pp. 2008–2011.

Ilknur Sur, Mine Altunbek, Mehmet Kahraman & Mustafa Culha. The influence of the surface chemistry of silver nanoparticles. *Nanotechnology*. 23(2012):37.pp 375102.

Iravani Siavash. Green synthesis of metal nanoparticles using plants. *Green Chem*. 13(2011).pp. 2638-2650.

Ivan Sondi & Branka Salopek-Sondi. Silver nanoparticles as antimicrobial agent: a case study on E. coli as a model for Gram-negative bacteria. *J. Colloid Interface Sci*. 275(2004):1.pp. 177–182.

Tian J, Wong KK, Ho CM, Lok CN, Yu WY, Che CM, Chiu JF & Tam PK. Topical delivery of silver nanoparticles promotes wound healing. *Chem. Med. Chem.* 2(2007).pp. 129-136.

Jeffrey N. Anker, W. Paige Hall, Olga Lyandres1, Nilam C. Shah1, Jing Zhao1 & Richard P. Van Duyn. Biosensing with plasmonic nanosensors. *Nature Materials.* **7**(2008).pp. 442–453.

Jung J.,Oh H., Noh H., Ji J. & Kim S. Metal nanoparticle generation using a small ceramic heater with a local heating area. *J. Aerosol. Sci.* 37(2006).pp. 1662-1670.

Khan Mohammad Ahsan Uddin, Arcot R. Lokanathan, Anna Liljeström, Xi Chen, Orlando J. Rojas & Janne Laine. Silver nanoparticle synthesis mediated by carboxylated cellulose nanocrystals. *Green Materials*. (2014).pp. 1-10.

Manash R. Das, Rupak K. Sarma, Ratul Saikia, Vinayak S. Kale, Manjusha V. Shelke & Pinaki Sengupta. Synthesis of silver nanoparticles in an aqueous suspension of graphene oxide sheets and its antimicrobial activity. *Colloids Surf., B*. 83(2011):1.pp. 16–22.

MedlinePlus. MedlinePlus Homepae [online]. 2013 [cited 13.30.2014] Protein electrophoresis – serum. Available in the Internet: http://www.nlm.nih.gov/medlineplus/ency/article/003540.htm

Mehta S. K., Bhawna Khushwinder Kaur & Bhasin K. K. Micellization behavior of cationic surfactant dodecyldimethylethylammonium bromide (DDAB) in the presence of papain. *Colloids Surf. A*. 317(2008):1-3.pp. 32-38.

Minwoo Park, Jungkyun Im, Mink wan Shin, Yuho Min, Jaeyoon Park, Heesook Cho, Soojin Park,Mun- Bo Shim, Sanghun Jeon, Da e-Young Chung, Jihyun Bae, JongjinPark, Unyong Jeong & Kinam Kim. Highly stretchable electric circuits from acomposite material of silver nanoparticlesand elastomeric fibres. *Nat. Nanotechnol*. 7(2012).pp. 803–809.

Mohd Abdul Majeed Khan, Sushil Kumar, Maqusood Ahamed, Salman A Alrokayan & Mohammad Saleh AlSalhi. Structural and thermal studies of silver nanoparticles and electrical transport study of their thin films. *Nanoscale. Res. Lett.* 6(2011):1.pp. 434.

Mustafa H. Chowdhury, Joseph R. Lakowicz & Krishanu Ray. Ensemble and single molecule studies on the use of metallic nanostructures to enhance the intrinsic

emission of enzyme cofactors. *J. Phys. Chem. C. Nanomater Interfaces.* 115(2011):15.pp. 7298-7308.

Nicolas Drogat, Robert Granet, Vincent Sol, Abdelmajid Memmi, Naïma Saad, Carmen Klein Koerkamp, Philippe Bressollier & Pierre Krausz. Antimicrobial silver nanoparticles generated on cellulose nanocrystals. *J. Nanopart. Res.* 13(2011):4.pp. 1557-1562.

Ockene IS, Chiriboga DE, Stanek EJ 3rd, Harmatz MG, Nicolosi R, Saperia G, Well AD, Freedson P, Merriam PA, Reed G, Ma Y, Matthews CE & Hebert JR. Seasonal variation in serum cholesterol levels: treatment implications and possible mechanisms. *Arch. Intern. Med.* 164(2004):8.pp. 863-870.

Lee P. C., Meisel D. Adsorption and surface-enhanced Raman of dyes on silver and gold sols. *J. Phys. Chem.*, 1982, 86 (17), pp. 3391–3395.

Pierre-Yves Silvert, Ronaldo Herrera-Urbina, Nicolas Duvauchelle, Venugopal Vijayakrishnan & Kamar Tekaia Elhsissen. Preparation of colloidal silver dispersions by the polyol process. Part 1—Synthesis and characterization. *J. Mater. Chem*., 6(1996).pp. 573-577.

Prashant V. Kamat, Mark Flumiani & Gregory V. Hartland. Picosecond dynamics of silver nanoclusters photoejection of electrons and fragmentation. J. *Phys. Chem. B*, 102(1998):17.pp. 3123–3128.

Tricker R. A. R. Introduction to meteorological optics. American Elsevier Publishing. New York, 1970. 225–229p.

Ren X, Meng X, Chen D, Tang F & Jiao J. Using silver nanoparticle to enhance current response of biosensor. *Biosens. Bioelectron*. 21(2005):3.pp. 433-437.

Ruggero Dondi, Wu Su, Gerry A. Griffith, Graham Clark & Glenn A. Burley. Highly size- and shape-controlled synthesis of silver nanoparticles via a templated tollens reaction. *Small.* 8(2012):5.pp. 770-776.

Rui Xiong, Canhui Lu, Wei Zhang, Zehang Zhou & Xinxing Zhang. Facile synthesis of tunable silver nanostrucutres for antibacterial application using cellulose nanocrytals. *Carbohydr. Polym*. 95(2013).pp. 214-219.

Sigma Corporation. Sigma product information sheet-trition x-100 [online]. [cited 24.07.2014]. Available in the Internet: http://www.snowpure.com/docs/triton-x-100-sigma.pdf

Son WK, Youk JH & Park WH. Antimicrobial cellulose acetate nanofibers containing silver nanoparticles. *Carbohydr Polym.* 65(2006):4.pp. 430–434.

Song J. Y., Jang H. K. & Kim B.S. Biological Synthesis of gold nanoparticles using Magnolia Kobus and Diopyros Kaki leaf extracts. *Process Biochem.* 44(2009).pp. 1133–1138.

Stephan T. Dubasa, Panittamat KumLangdudsana & Pranut Potiyaraj. Layer-by-layer deposition of antimicrobial silver nanoparticles on textile fibers. *Colloids Surf. A*. 289(2006):1-3.pp. 105–109.

Takeshi Tsuji, D.-H. Thang, Yuuki Okazaki, Masataka Nakanishi, Yasuyuki Tsuboi & Masaharu Tsuji. Preparation of silver nanoparticles by laser ablation in polyvinylpyrrolidone solutions. *Appl. Surf. Sci.* 254(2008):16.pp. 5224–5230.

Tas A. Cuneyt. The use of physiological solutions or media in calcium phosphate synthesis and processing. *Acta Biomate.*. 10(2014):5.pp. 1771-92.

Tolaymat T.M., A.M. Badawy, A. Genaidy, K.G. Scheckel, T.P. Luxton & M. Suidan. An evidence-based environmental perspective of manufactured silver nanoparticle in syntheses and applications: a systematic review and critical appraisal of peer-reviewed scientific papers. *Sci. Total Environ.* 408(2010):5.pp. 999-1006.

Kreibig U. & Vollmer M. Optical properties of metal clusters, Springer. Berlin, 1995.

Vodnik VV, Bozanić DK, Bibić N, Saponjić ZV & Nedeljković JM. Optical properties of shaped silver nanoparticles. *J. Nanosci. Nanotechnol.* 8(2008):7.pp. 3511-3515.

Wei H., Chen C., Han B. & Wang, E. Enzyme colorimetric assay using unmodified silver nanoparticles. *Anal. Chem.* 80(2008).pp. 7051–7055.

Xia Younan, Xiong Yujie, Lim B & Skrabalak SE. Shape-controlled synthesis of metal nanocrystals: simple chemistry meets complex physics? *Angew. Chem. Int. Ed. Engl.* 48(2009):1.pp. 60-103.

Xia Xiaohu, Li Weiyang, Zhang Yu & Xia Younan. Silica-coated dimers of silver nanospheres as surface-enhanced Raman scattering tags for imaging cancer cells. *Interface Focus*. 3(2012):3.pp. 20120092.

Xiu ZM, Zhang QB, Puppala HL, Colvin VL & Alvarez PJ. Negligible particle-specific antibacterial activity of silver nanoparticles. *Nano. Lett*. 12(2012):8.pp. 4271-4275.

Meng Yanjing, Lai Yongchao, Jiang Xiaohong, Zhao Quanqin & Zhan Jinhua. Silver nanoparticles decorated filter paper via self-sacrificing reduction for

membrane extraction surface-enhanced Raman spectroscopy detection. *Analyst*. 138(2013).pp. 2090-2095.

Yi Fu, Jian Zhang & Joseph R. Lakowicz. Large enhancement of single molecule fluorescence by coupling to hollow silver nanoshells. *Chem. Commun. (Camb)*. 48(2012):78.pp. 9726-9728.

Yu A Krutyakov, A A Kudrinskiy, A Yu Olenin & G V Lisichkin. Synthesis and properties of silver nanoparticles: advances and prospects. *Russian Chemical Reviews* 77(2008):3.pp. 233-257.

Zhang Zhiqiang, Ramesh C. Patel, Rajshree Kothari, Colin P. Johnson & Stig E. Friberg. Stable silver clusters and nanoparticles prepared in polyacrylate and inverse micellar solutions. *J. Phys. Chem. B*. 104 (2000):6.pp. 1176–1182.